Extensive studies on CeF_3 crystals a good candidate for electromagnetic calorimetry at future accelerators

E. Auffray, S. Baccaro, T. Beckers, Y. Benhammou, a N. Belsky, B. Borgia, D. Boutet, R. Chipaux, I. Dafinei, F. de Notaristefani, et al.

EUROPEAN ORGANIZATION FOR NUCLEAR RESEARCH

CERN–PPE/96–064
26 March 1996

EXTENSIVE STUDIES OF CeF_3 CRYSTALS, A GOOD CANDIDATE FOR ELECTROMAGNETIC CALORIMETRY AT FUTURE ACCELERATORS

E.Auffray[1], S.Baccaro[2], T.Beckers[3*], Y.Benhammou[4], A.N.Belsky[5], B.Borgia[6], D.Boutet[7], R.Chipaux[8], I.Dafinei[1**], F.deNotaristefani[6], P.Depasse[4], C.Dujardin[7], H.ElMamouni[4], J.L.Faure[8], J.Fay[4], M.Goyot[4], S.K.Gupta[9], A.Gurtu[9], H.Hillemanns[10], B.Ille[4], T.Kirn[10], M.Lebeau[11], P.Lebrun[4], P.Lecoq[1], J.A.Mares[12], J.P.Martin[4], V.V.Mikhailin[5], B.Moine[7], J.Nelissen[3], M.Nikl[12], C.Pedrini[7], R.Raghavan[9], P.Sahuc[4], D.Schmitz[10], M.Schneegans[11], J.Schwenke[10], S.Tavernier[3], V.Topa[13], A.N.Vasil'ev[5], M.Vivargent[11], J.P.Walder[4]

Abstract

In the framework of its search for new heavy, fast, and radiation-hard scintillators for calorimetry at future colliders, the Crystal Clear Collaboration performed a systematic investigation of the properties and of the scintillation and radiation damage mechanisms of CeF_3 monocrystals. Many samples of various dimensions up to $3\times3\times28 cm^3$ were produced by industry and characterized in the laboratories by different methods such as optical transmission, light yield and decay time measurements, excitation and emission spectra, gamma and neutron irradiations. The results of these measurements are discussed. The measured light yield is compared with the theoretical expectations. Tests in high-energy electron beams on a crystal matrix were also performed. The suitability of CeF_3 for calorimetry at high-rate machines is confirmed. Production and economic considerations are discussed.

(Submitted to Nuclear Instruments and Methods in Physics Research)

This work was performed in the framework of The Crystal Clear Collaboration (RD18)

[1] CERN, Geneva, Switzerland.
[2] ENEA Casaccia, INFN Rome, Italy.
[3] VUB, Vrije Universiteit Brussels, Belgium.
[4] IPN of Lyon, IN2P3-CNRS and Université Claude Bernard, Villeurbanne, France.
[5] Synchrotron Radiation Laboratory, Moscow State University, Moscow, Russian Federation.
[6] INFN Rome, Italy.
[7] LPCML of Lyon, CNRS and Université Claude Bernard, Villeurbanne, France.
[8] CEA DSM/DAPNIA, CE-Saclay, France.
[9] Tata Institute of Fundamental Research, Bombay, India
[10] Physics Institute, RWTH Aachen, Germany.
[11] LAPP, IN2P3-CNRS, Annecy-le-Vieux, France.
[12] Institute of Physics, Academy of Sciences of Czech Republic, Prague, Czech Republic.
[13] Institute of Atomic Physics (IFA) Bucharest, Romania.
[*] Now at UIA, Universitaire Intselling, Antwerp, Belgium.
[**] On leave from Institute of Atomic Physics (IFA) Bucharest, Romania.

1. INTRODUCTION

In several fields of physics and industry, the need for a new generation of inorganic scintillators is more and more often expressed. For instance, low- and high-energy physics, astrophysics, medical imaging (PET scanners, cameras for mammography, etc.) and some industrial applications would greatly benefit from heavier crystals with larger and faster light output, better radiation resistance, and lower cost than those currently in use.

The following characteristics are required in particular in calorimetry at future particle factories and high-energy colliders, such as the Large Hadron Collider (LHC) at CERN: high density ($>5 g/cm^3$) for fine granularity and compactness of the detector, good optical transmission for light collection uniformity in long crystals, sufficient light yield for excellent energy resolution, short scintillation decay time for collecting most of the light in less than 100ns, good resistance to radiations with gamma dose rates approaching 1Mrad/yr and neutron fluences of about $10^{13} n/cm^2$, and cost below $\$2/cm^3$ since volumes of several tens of cubic metres are foreseen.

An R&D collaboration, the 'Crystal Clear Collaboration' (CCC, CERN/RD18), was set up [1] in order to coordinate the efforts of many laboratories and firms in finding and producing such scintillators. The laboratories essentially perform the characterization of the samples by various methods: optical transmission measurements, light yield and decay time measurements, excitation and emission spectra. Some laboratories have special equipment such as a synchrotron radiation source (LURE) for spectroscopy, ^{60}Co sources and reactors for gamma and neutron irradiations (DAPNIA Saclay, TIFR Bombay, ENEA Casacia Rome, CERN) or high-energy electron beams for energy resolution measurement (CERN). The samples are produced by industry; 23 firms agreed to collaborate with the CCC in producing small samples, or successive samples of a particular crystal in limited development programmes, or series of long crystals.

The Crystal Clear Collaboration investigated several families of crystals chosen for their potential for fast scintillation and radiation hardness. Fluorides, similar to BaF_2, such as CeF_3, LaF_3, PbF_2, looked promising in this respect. Ternary fluoride compounds were expected to have similar optical properties and could lead to heavy matrices such as BaY_2F_8, $KMgF_3$, $LiYF_4$, $ErYF_4$. Heavy fluoride glasses were expected to have similar characteristics at what was hoped to be a lower cost and therefore deserved special efforts. Some oxides, such as cerium-doped orthosilicates (GSO, LSO) and aluminium-based perovskites (YAP:Ce, GAP:Ce, LuAP:Ce) seemed very attractive when high light yield is important.

Among the crystals already known in 1990, cerium fluoride, with its short radiation length, small Molière radius and fast response, seemed one of the best candidates for high-energy calorimetry. Some crystals are denser, such as BGO, PbF_2 or $PbWO_4$, but BGO is too slow, $PbWO_4$ has a poor scintillation light yield and PbF_2 is only a Cherenkov radiator. Crystals such as pure CsI and BaF_2 are fast but have marginal densities and exhibit slow components.

Since CeF_3 seemed to have the required qualities for calorimetry and had no serious known drawbacks, the CCC undertook an extensive study of its characteristics and of the mechanisms of its luminescence and possible damage under irradiation. Furthermore, the best conditions for a stable high-quality mass production were explored.

2. GENERAL FEATURES OF CeF_3

In 1989, Anderson [2], and Derenzo and Moses [3] discovered independently the fast scintillation properties of CeF_3 on small samples of a few cm^3. These properties, in addition to a relatively high density and light yield as measured on the tested samples, made this crystal very attractive for high rate applications.

At that time, except for the crystallographic structure [4,5] and the general properties which are summarized in Table1, little was known about the fundamental properties of CeF_3 such as the origin of its scintillation, its radiation hardness, or the possibility to grow crystals of suitable size for building an electromagnetic calorimeter.

Table 1

General properties of CeF_3

Density	$6.16 g/cm^3$
Radiation length	1.68 cm
Molière radius	2.63 cm
Light yield	55 (% BGO)
Decay time	5 ns (fast component) 30ns (slow component)
Emission peak	286, 300, 340nm
Refractive index at 310nm	1.63
Melting temperature	1443 °C
Hygroscopicity	None

For this reason, since 1990, the Crystal Clear Collaboration has undertaken a thorough evaluation of the properties of CeF_3 [1]. In only four years, the number of crystal grower companies involved in this development went from one (Optovac) to eight, the size of the crystals increased from a few cm^3 to more than $250 cm^3$, and the crystal quality improved considerably.

3. EXPERIMENTAL CONDITIONS AND METHODS

3.1 Crystal samples

More than 350 samples grown by eight different producers from all over the world (see Table2) and using different raw materials have been studied. All crystals were grown using the Bridgman method. Some crystals were doped with divalent (e.g. barium) or tetravalent cations (e.g. hafnium, zirconium). Each crystal has an identification number which is referenced in some of the results presented below.

Table 2
List of CeF_3 producers collaborating with Crystal Clear

Producer	Town, country	Samples
BGRI	Beijing, China	16
Crismatec	Grenoble, France	19
Karl Korth	Kiel, Germany	28
Crytur	Turnov, Czech Rep.	47
NKK	Tatebayashi-ci, Japan	35
Optovac	North Brookfield, USA	192
SIC	Shanghai, China	6
SOI, Sorem	Pau, France	14

3.2 Optical transmission measurements

The optical transmission spectra of crystals in the range 200–700nm were measured before and after irradiation on a spectrophotometer built at CERN [6], using a 150W xenon lamp and a Jobin-Yvon H20UV monochromator with a 2nm resolution.

From the transmission measurements, the intrinsic or induced absorption coefficient was obtained using the relation

$$\mu = \left(\frac{1}{L}\right) \times \ln\left(\frac{T_0}{T}\right)$$

where μ is the intrinsic absorption coefficient if T_0 is the theoretical transmission and T the measured transmission, or μ is the radiation-induced absorption coefficient if T_0 is the transmission before irradiation and T the transmission after irradiation. L is the crystal length in metres.

3.3 Fluorescence measurements

Excitation and emission spectra were recorded on a JY3D (Jobin-Yvon) spectrofluorimeter built around two H20 UV monochromators, and on a 199S spectrofluorimeter (Edinburgh Instrument [7]). The UV synchrotron radiation from the SUPERACO storage ring at LURE (Orsay, France) through a 3 metre vacuum-UV monochromator was also used as a light source [8].

3.4 Decay kinetics measurements

The photoluminescence decay curves were measured by the single-photon counting method with a 199S spectrofluorimeter (Edinburgh Instrument), and fluorescence decay times were obtained from the decay curves using the common deconvolution procedure.

The scintillation decay time is measured by the delayed coincidence method [9]. A β^+ ^{22}Na source excites both a fast plastic scintillator and the crystal. The delayed signal from the plastic scintillator coupled to a photomultiplier tube gives the start signal, and a second photomultiplier tube placed at 10cm from the scintillating crystal and working in the photon counting mode gives the stop signal. The signals, processed through constant fraction discriminators and an Ortec 566 time-to-amplitude converter, are analysed on a Tracor-Northern TN-7200 multichannel analyser. The decay time at different wavelengths can be measured by

placing a monochromator between the crystal and the second photomultiplier. The decay curves obtained can be used after corrections to construct the radioluminescence spectrum.

3.5 Light yield measurements

The light yield (LY) measurements refer to the amount of light collected on the photocathode of a photomultiplier or on the sensitive area of a photodiode. No attempt has been made to correct for sample shape or volume. For these measurements, the crystals were wrapped in aluminized Mylar or Millipore [10] and optically coupled to a quartz window XP2020Q Philips photomultiplier (PM) by a 47V Rhodorsil Rhône-Poulenc optical oil. The fluorescence produced by gamma rays from a ^{137}Cs radioactive source is detected by the PM and the signal is processed by a Borer type CERN N2620 shaping amplifier and analysed on a Silena multichannel analyser.

3.6 Irradiation sources

Most of the cerium fluoride crystals were irradiated with the ^{60}Co source (4400Ci, 2Gy/min) at the radiotherapy unit of the Geneva Cantonal Hospital. Some crystals were also irradiated at the Calliope ^{60}Co source at ENEA near Rome, Italy (66Gy/min). Low dose-rate measurements were performed on some samples using the 680mCi Cobalt source (0.02Gy/hour) of the DEIN, CE Saclay, France [11].

Irradiation at low temperature was performed with an electron beam of 7MeV at the Linear Accelerator Facility of the Institute of Atomic Physics in Bucharest, Romania, at dose rates ranging from 0.1×10^3 to 1.6×10^3rad/s [12].

For neutron irradiations, some samples were irradiated in a uniform neutron flux inside the 300kW nuclear reactor ASPARA at the Bhabha Atomic Research Centre in Bombay, India [13] and other samples in the Ulysse reactor of INSTN, Saclay, France [14]. The fluence varied from 10^9 to 10^{14}n/cm^2.

4. OPTICAL PROPERTIES

4.1 Optical transmission and intrinsic absorption

4.1.1 Generalities

The transmission curve generally reflects the optical quality of the crystal. In order to compare the optical quality from crystal to crystal, the transmission of all the samples has been measured from 200nm to 700nm and compared with the theoretical transmission calculated using the Sellmeier equation [15]. As illustrated in Fig.1, for some crystals (CF30, CF164) from the initial period of production, the transmission differs significantly from the theoretical transmission. It has been shown that the absorption peaks observed in the transmission spectra of the CF30 sample are caused by the presence of a high concentration of neodymium (200ppm), and for sample CF164 the large band at 350nm has been attributed to the high concentration of oxygen [16]. These elements are the impurities most often present in CeF_3. After improving the raw materials and in particular reducing the oxygen concentration, all producers succeeded in growing small CeF_3 samples with a transmission close to theoretical as shown for CF130 [16].

While the transmission is similar for most samples, between 350nm and 700nm, the optical absorption edge varies by about 15nm between undoped crystals grown from high-purity raw material and crystals doped with a divalent cation such as barium (Fig.2) [16,17].

This variation is attributed to the increase of the crystal field in the presence of impurities (oxygen or fluorine vacancies) near the Ce^{3+} ions. This leads to a stretching of the 5d energy bands, which subsequently results in a smaller band gap between the lowest 5d level and the 4f fundamental levels and therefore in a shift to lower energies of the optical absorption edge for the doped crystals.

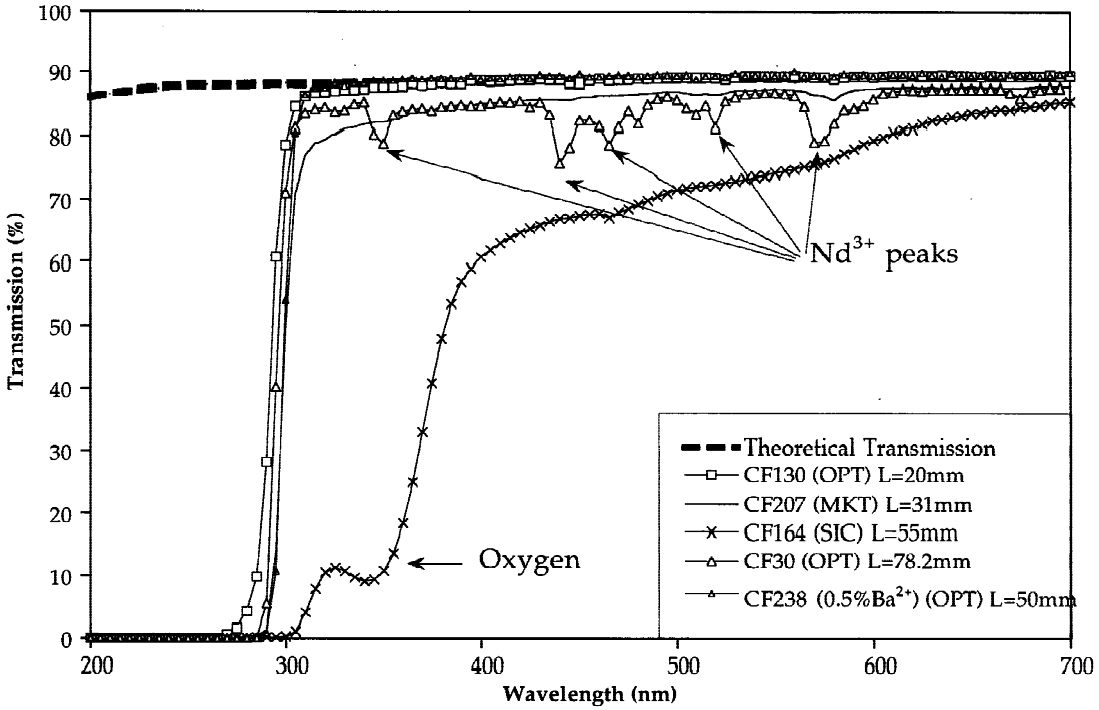

Fig. 1: Comparison of longitudinal transmission of different quality CeF_3 crystals with the theoretical transmission

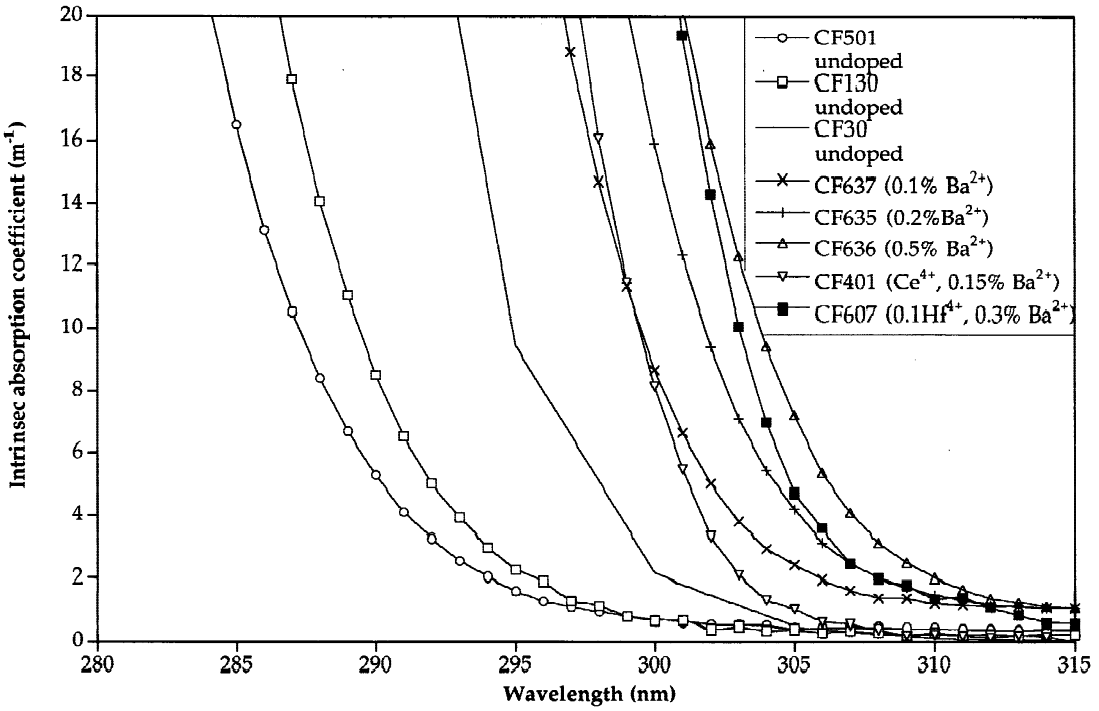

Fig. 2: Intrinsic optical absorption edge for different CeF_3 crystals

4.1.2 Production of long crystals

At the start of the production of long crystals, it was very difficult to grow scatter-free undoped crystals; only the crystals doped with divalent cations were transparent. The first undoped crystals presented either some white scatter generally oriented at 45° of the *c*-axis or were clear but presented a large dispersion of the optical absorption edge along the length of the crystal with a redshift on the seed side (Fig.3a). These two facts (white scatters and dispersion of the optical absorption edge) have been attributed to the presence of oxygen, difficult to suppress in fluorides [16].

Thanks to an important effort in the preparation of the raw materials, particularly in the reduction of oxygen contamination, several long and scatter-free undoped CeF_3 crystals from different producers were available at the end of 1994 with a longitudinal transmission close to theoretical. Moreover, the very small dispersion (< 1nm) of the optical absorption edge shows that the quality of crystals is now well controlled along the entire crystal length (Fig.3b).

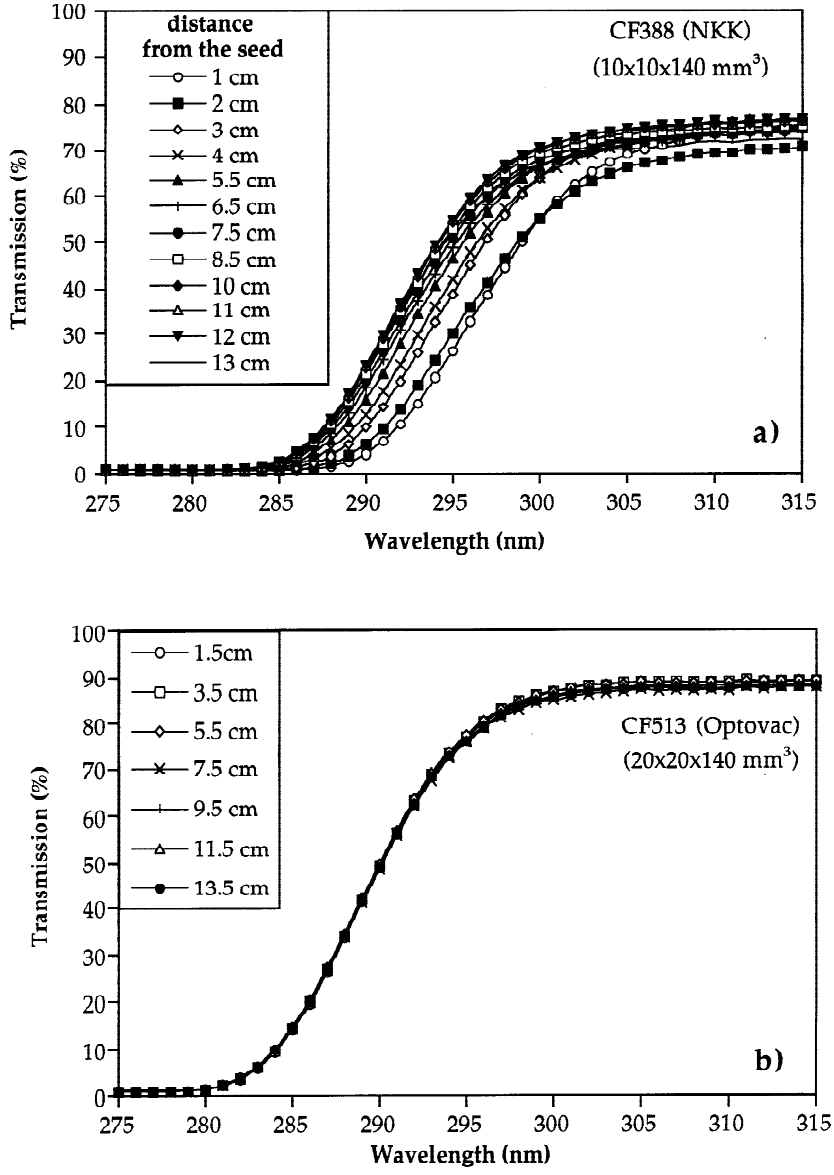

Fig. 3: Transversal transmission spectra measured at several points along the crystal: a) for a crystal received earlier; b) for a recently received crystal

The progress in the production of large crystals is illustrated on Fig.4 where the evolution in quality of the optical transmission of the crystals produced by NKK over two years is presented. While the first crystals had a transmission below 40% due to the presence of white scatters, most recent samples, even if they still present a slight absorption at 350nm, have a transmission near to the theoretical transmission. Four years' work on the production of large crystals showed that it is possible to grow CeF_3 crystals with the dimensions and the optical quality required for application in high-energy physics.

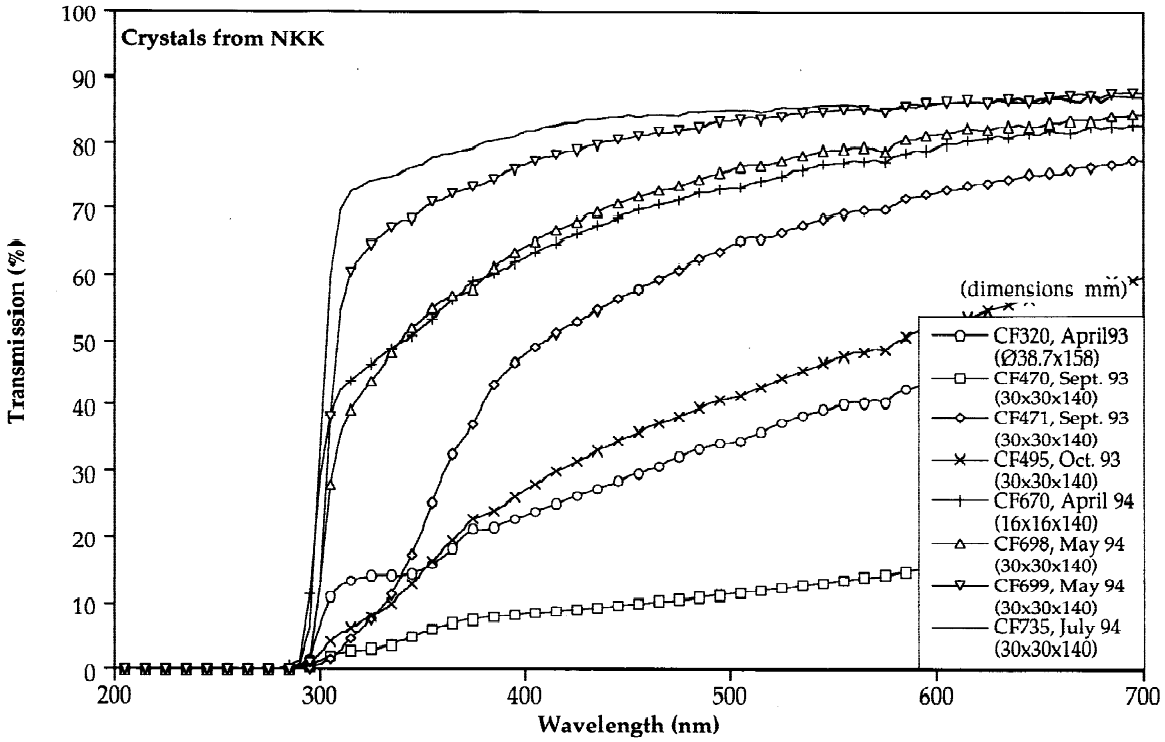

Fig. 4: Optical transmission evolution of CeF_3 crystals produced by NKK

4.2 Luminescence properties

In 1989, after the discovery of the scintillation properties of CeF_3 [2,3], the spectroscopy and the origin of its luminescence were not really known [18,19]. Thanks to the intensive work of several groups from the collaboration [7,8,20–22] as well as of other groups [23], the spectroscopy of CeF_3 is now well understood.

4.2.1 Photoluminescence

The luminescence of CeF_3 is due to the transition from the lowest excited Ce^{3+} 5d level to the ground 4f level, split by the spin-orbit coupling (see Fig.12b for energy levels) [8,20]. Different cerium sites participate in the emission mechanism: regular cerium with emission bands at 286nm and 305nm and cerium at perturbed sites with a broad emission band at 340nm. The emission spectra of CeF_3 samples depend on the number of perturbed sites, and therefore on the crystal quality (Fig.5). The origin of the perturbation of some Ce^{3+} ions is attributed to defects close to them, principally fluorine vacancies or oxygen [22]. Owing to the reduction of these defects in recent crystals, the concentration of Ce^{3+} ions in perturbed sites is low, and the photoluminescence spectrum is similar to that of crystal CF557 on Fig.5.

Both radiative and non-radiative energy transfer processes from the regular to perturbed Ce^{3+} were made evident [21,22] as well as the influence of near surface trap states [8]. The transfer is essentially radiative for crystals with a low concentration of perturbed Ce^{3+} [21] and non-radiative in the case of a high concentration [22]. This explains the different forms of Ce^{3+} decay observed in photoluminescence.

For crystals with less emission from perturbed sites, the decay time spectrum for direct excitation for both regular and perturbed Ce^{3+} (respectively at 250nm and 286nm) is exponential with a decay time of about 20ns for regular and 30ns for perturbed Ce^{3+} [7,21]. When perturbed ions are excited at 250nm, the decay curve shows a non-negligible rise time due to the radiative energy transfer from regular to perturbed Ce^{3+} ions (Fig.6) [21]. For crystals presenting an intense emission band at 340nm, the decay curve with direct excitation for regular Ce^{3+} is non-exponential with a mean decay time of a few ns, strongly dependent on temperature [22]. It is due to the existence of a non-radiative energy transfer mechanism from regular to perturbed Ce^{3+}, attributed to the dipole–dipole interaction between the ions [22]. When exciting the perturbed Ce^{3+}, the decay curve is slightly non-exponential with a mean decay time around 30ns. The non-exponential behaviour has been attributed to a concentration quenching of perturbed Ce^{3+} (Fig.7) [22].

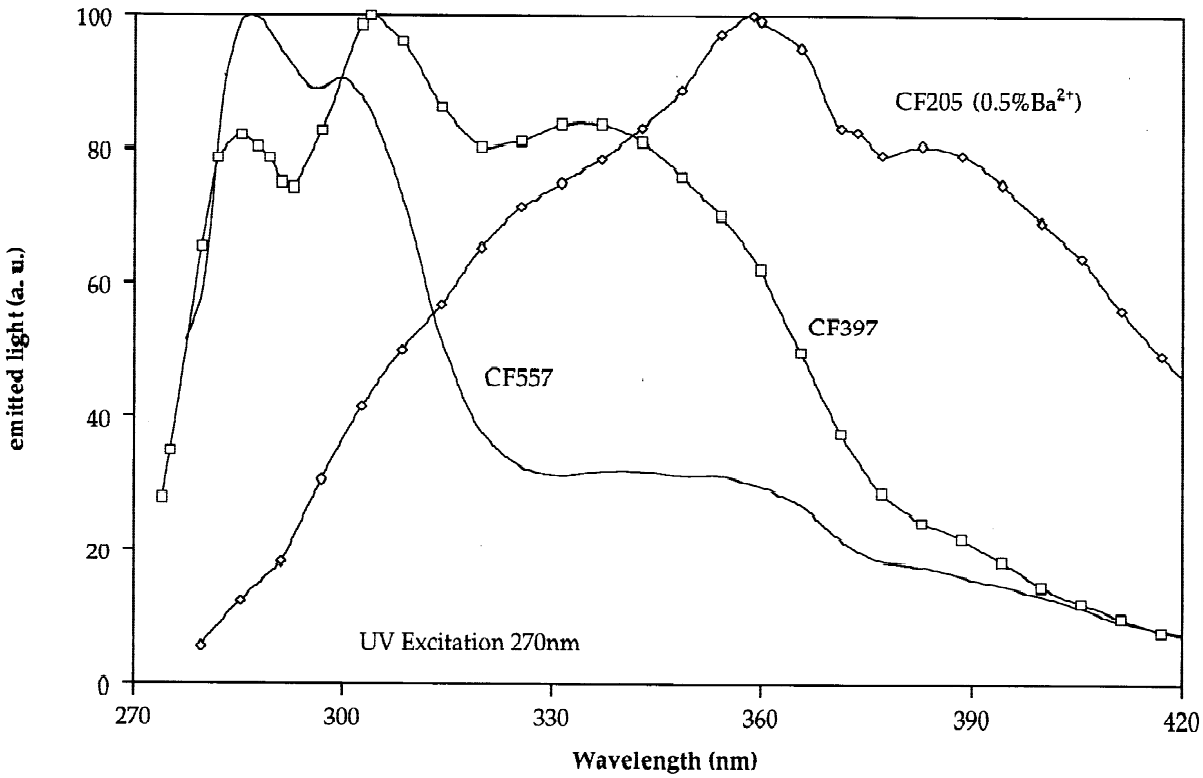

Fig. 5: Photoluminescence spectra for different CeF_3 crystals

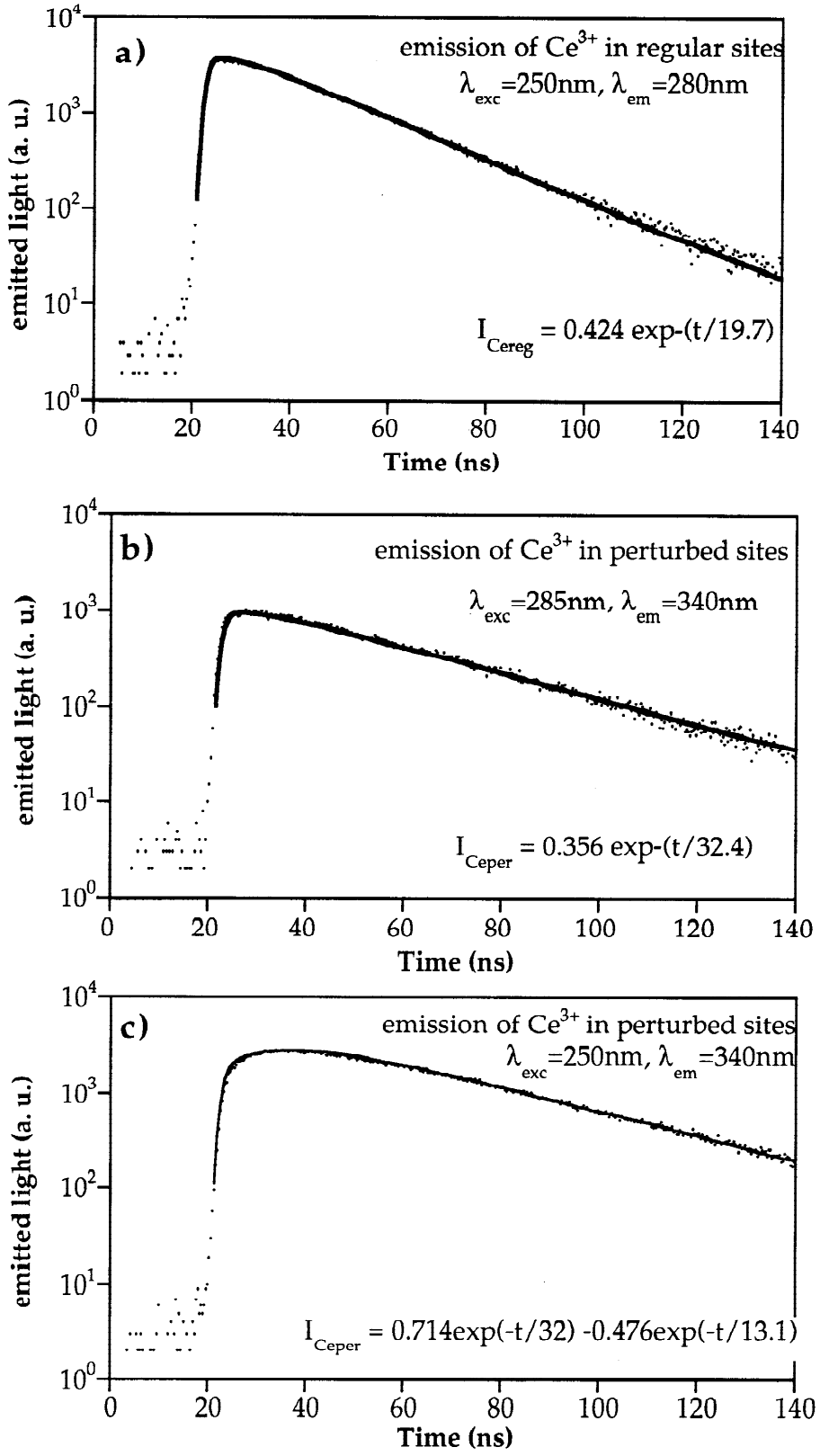

Fig. 6: Decay curves for different excitation and emission wavelengths for a CeF_3 crystal (CF159 from Optovac). The coefficient of the exponentials in the formula are obtained by deconvoluting the instrumental response from the experimental curve; instrumental response is not given in figure

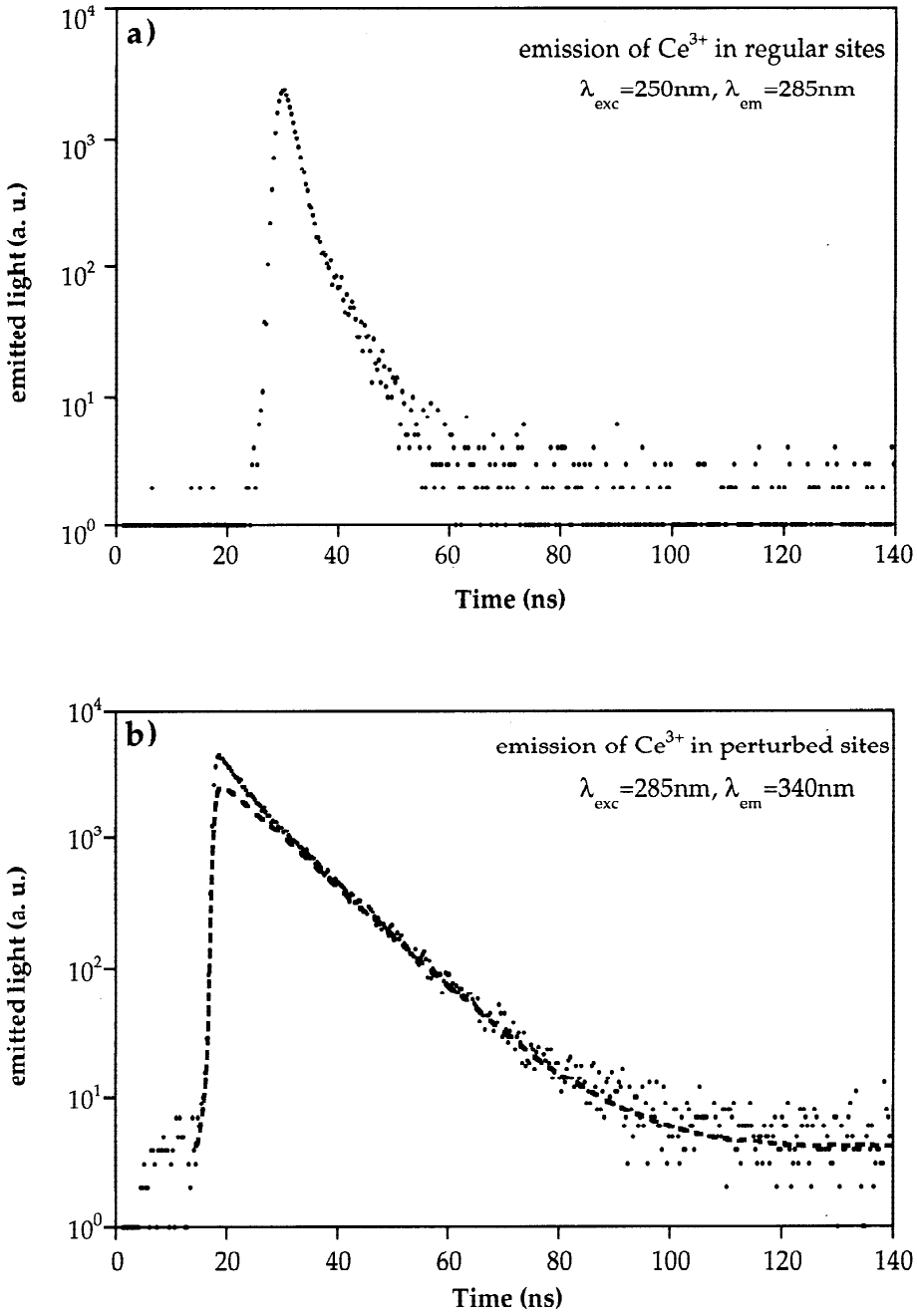

Fig. 7: Decay curves at different wavelengths for a Cd^{2+} doped crystal [from Vavilov State Optics Institute (SOI)]

4.2.2 Radioluminescence

When the crystal is excited by gamma rays (radioluminescence), the emission spectrum presents some differences from the photoluminescence spectrum (Fig.8). The peak at 286nm is not present and the intensity of the band at 340nm is much reduced. Since the excitation takes place in the bulk of the crystal, the light emitted at 286nm is reabsorbed by the lattice (see transmission curves). The decrease in intensity of the band at 340nm is due to the lower concentration of Ce^{3+} in the bulk of the crystal rather than near the surface. In fact, the quality near the surface is strongly dependent on cutting, polishing, and storage conditions.

Under γ excitation, whatever the concentration of perturbed cerium, the decay of regular Ce^{3+} is strongly non-exponential in contrast with the photo-excitation (Fig.9). This effect was noticed for X-ray synchrotron excitation [24] and later it was shown that the decay under γ (511keV) excitation can be approximated by a sum of 3 exponentials [25]. The shape of the decay curve for γ excitation reveals the presence of a non-radiative process of de-excitation. The temperature dependence of the decay process was also noticed [25]. An explanation of this process, based on the hypothesis of the existence of a dipole–dipole interaction between close lying regular excited Ce^{3+}, has been proposed:

$$(Ce^{3+})^* + (Ce^{3+})^* \rightarrow Ce^{3+} + Ce^{4+} + e^- .$$

This interaction results in the loss of two emission photons, as a free electron created in the conduction band has a very small probability of radiative recombination with a Ce^{4+} hole centre [23].

It has been shown that the multiexponential nature of the decay of regular Ce^{3+} can be perfectly explained with this interpretation [25] taking into account the space distribution of Ce^{3+} sites in the CeF_3 lattice.

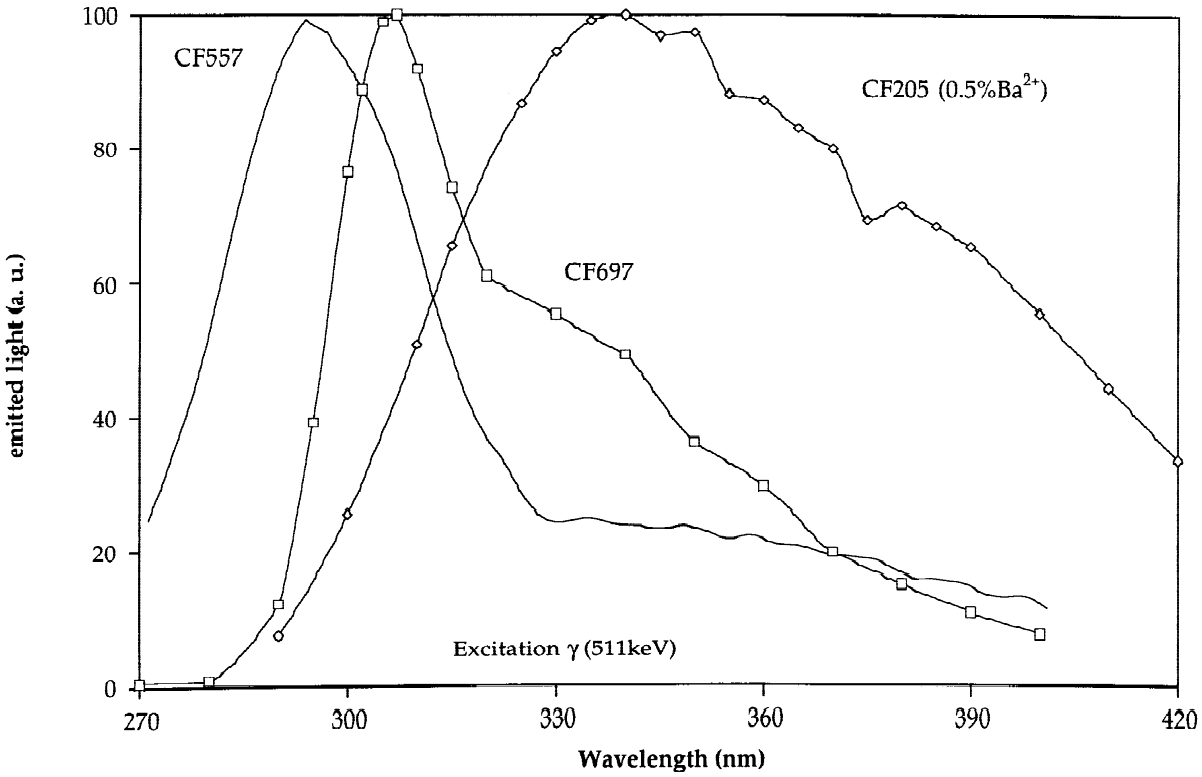

Fig. 8: Radioluminescence spectra of different CeF_3 crystals

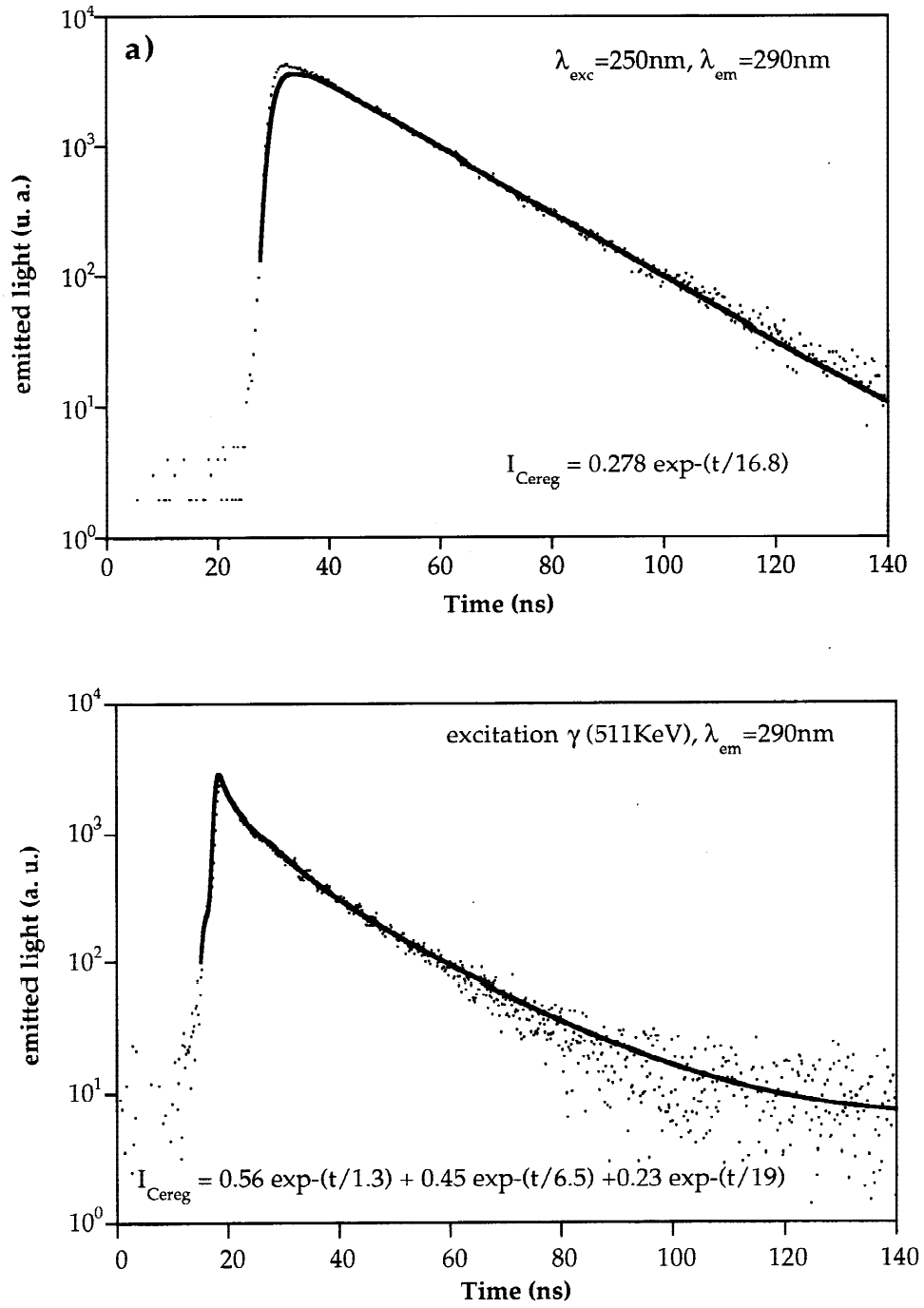

Fig. 9: Decay curves for Ce^{3+} ion in regular site (CF557 from Optovac): a) under direct 250nm excitation; b)under gamma excitation. The coefficient of the exponentials in the formula are obtained by deconvoluting the instrumental response from the experimental curve; instrumental response is not given in figure

4.2.3 Light production

A strong correlation between the position of the optical absorption edge and the scintillation light yield has been observed. Comparing crystals of the same dimensions, barium doping results in a light yield 1.5times less than in pure CeF_3 crystals (Fig.10), and corresponds to a shift to the red of the optical absorption edge of about 15nm. When the optical absorption edge is above 300nm, a part of the emission and particularly the emission of regular Ce^{3+} (286nm and 305nm) is absorbed by the crystal and lost for detection [16,26].

For a good quality CeF_3 crystal, the maximal value obtained for a volume of $2\times2\times2cm^3$ is 2100photons/MeV (value confirmed by other groups [23,27]). For a long crystal of the same optical quality, this corresponds to a measured light yield of 1200–1400photons/MeV [16,17,26].

The dependence of light yield on temperature has been measured (Fig.11), from –200°C to 100°C [16]. In the room-temperature region, this variation is only 0.14%/°C. This low variation is important for the construction of a large calorimeter with more than 100000 crystals and electronic channels. No sophisticated temperature control system is needed.

The fraction of collected light measured as a function of time, for crystals of different sizes and grown by different manufacturers, is very constant from crystal to crystal and shows for instance that within 25ns (one LHC bunch-crossing interval) 55% of the light can be collected [16,26].

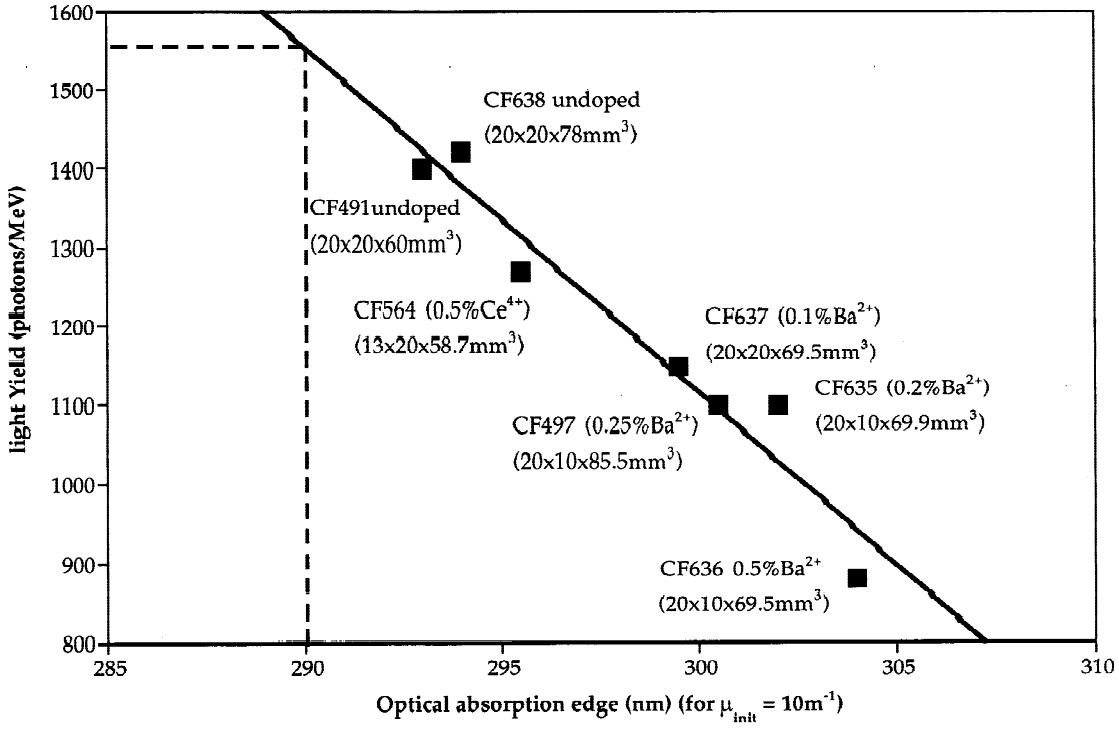

Fig. 10: Correlation between light yield and optical absorption edge

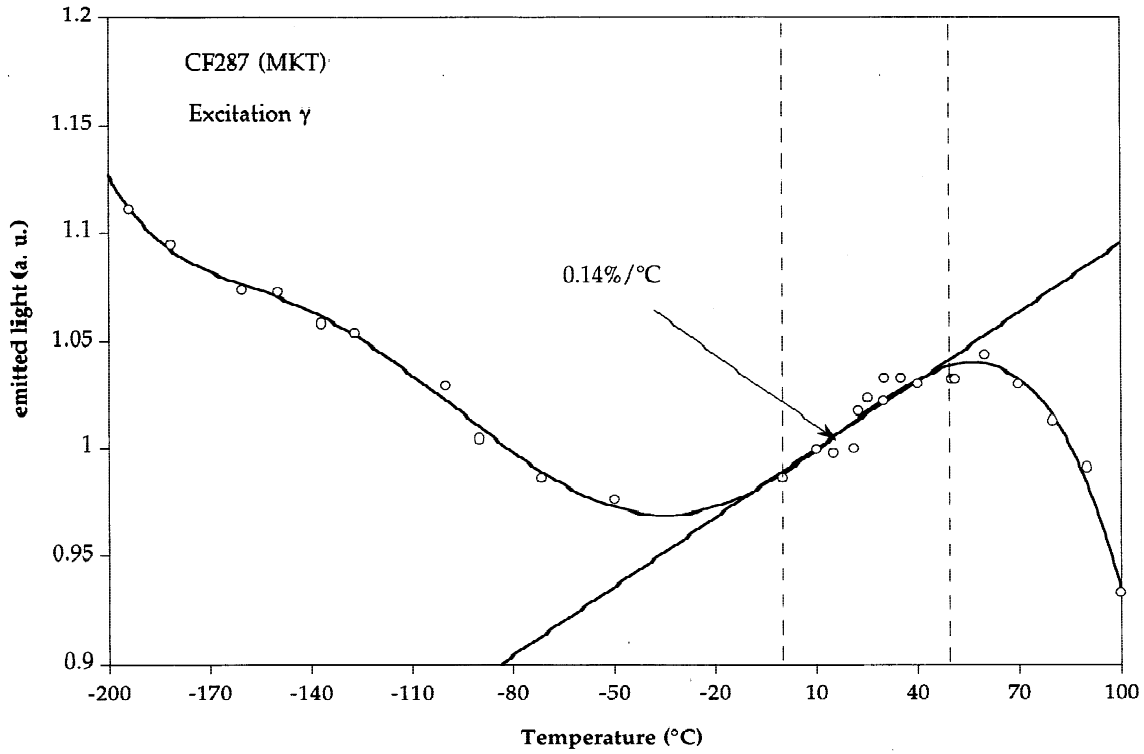

Fig. 11: Dependence of light yield on temperature

4.3 Discussion on the scintillation

The light yield values reached by the new generation of CeF_3 crystals are sufficient to ensure that the energy resolution of a CeF_3 calorimeter would not be limited by photostatistics. But these values are quite low in comparison with theoretical predictions, even if we take into account the light lost by non-radiative de-excitation processes [25] estimated to be between 40% and 60%.

During recent years (1991–95), the scintillation mechanism of CeF_3 has been studied intensively [8,20,24,25,27–32] in order to understand why it exhibits a much lower light output (1500–4500photons per MeV) under high-energy excitation than the estimated conversion limit value of about 25000photons per MeV.

Furthermore, this simple crystal is an interesting model for the investigation of the energy relaxation and transfer mechanisms from excited states. This kind of relaxation includes the multiplication of electronic excitations due to inelastic scattering of electrons and Auger relaxation of holes, the interaction between the resulting secondary excitations, the surface quenching due to the propagation of excitations to the surface, and the correlated recombination of electrons and holes with production of the pre-radiative states.

A good approach for studying such phenomena is synchrotron radiation spectroscopy. The synchrotron (pulsed and monochromatized) excitation source emitting in the vacuum ultraviolet (VUV) and X-ray range is an ideal tool for selective creation of some of these excited states and for the analysis of the dynamics of the process. After the absorption of a gamma-quantum with energy around 1MeV, fast electrons mainly excite the highest lying electron levels in Ce^{3+} with energy of 10–100eV, since the energy loss function is large in this energy region. Therefore VUV radiation, which can directly excite these levels, gives an opportunity to study the important stage of energy transport and relaxation in the scintillation processes.

4.3.1 Experimental results

Reflectivity and fluorescence excitation spectra and fluorescence decay time spectra of CeF_3 and LaF_3:Ce have been recorded and analysed in the VUV range up to 120eV and in the X-ray region [31,33]. Figure12a shows the excitation and absorption spectra of CeF_3. The absorption spectrum at low energies is deduced from data of weakly doped LaF_3 [32], while above 9eV it is calculated from reflectivity data using the Kramers–Kronig relations. The anticorrelation between peaks of fluorescence yield and absorption in the low-energy range is due to the surface quenching effect which has been studied in detail [32]. The reduction of the quantum yield due to surface losses is estimated to be about 10–60% of the volume yield for excitation photon energy in the range 10–40eV. The amount of surface losses modifies only slightly the shape of the excitation spectrum.

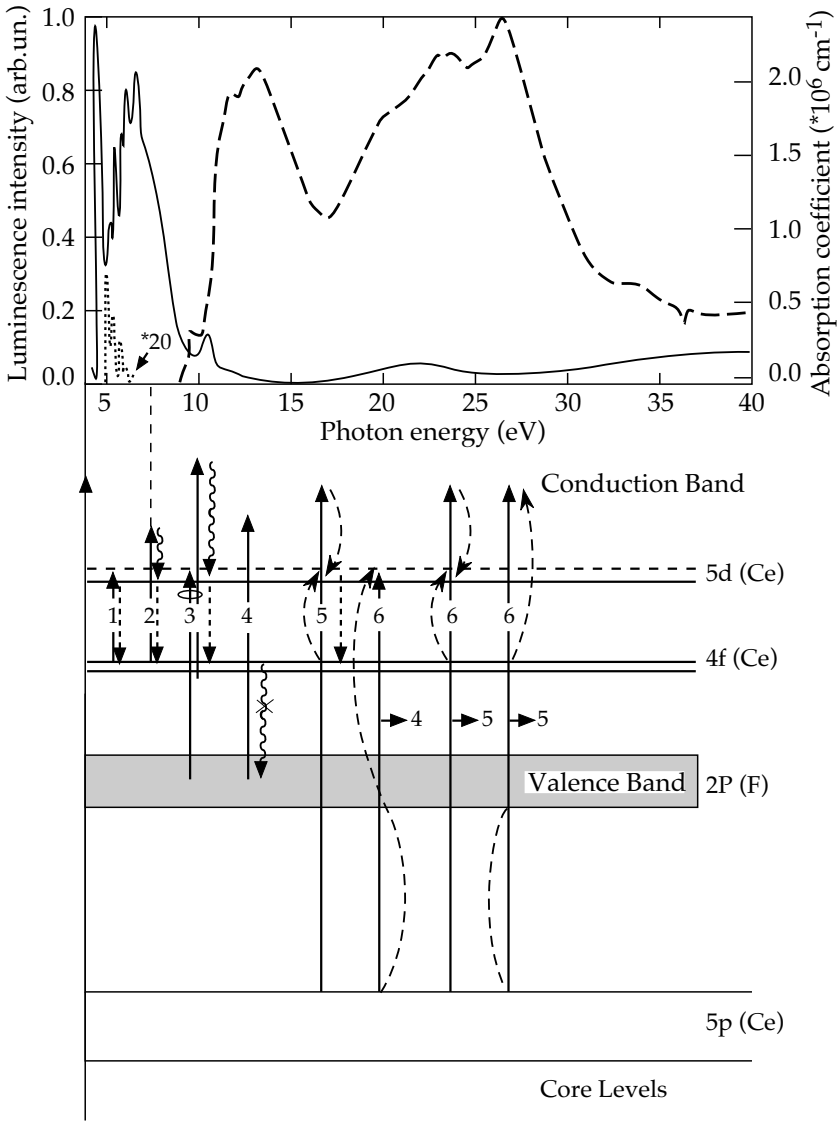

Fig. 12: a) Excitation (full curve, emission: 300 nm) and absorption (dotted curve) spectra of CeF_3 at room temperature; b) CeF_3 band structure scheme where the dominant processes occurring at various excitation energies are sketched. The straight full lines are for excitation transitions, straight dashed lines are for emission transitions, wavy lines show non-radiative relaxations, and curved dashed lines represent Auger Fano process. The processes marked by vertical arrows are related to photon energy directly above in Fig. 12a (see process 2)

Figure12b shows the band structure of CeF_3 deduced from X-ray photoelectron spectroscopy [34,35]. The energy gap between the top of the valence band formed by the 2p electrons of F^- ions and the conduction band is about 10eV and the energy of the partly filled 4f Ce^{3+} level is 4.5eV above the top of the valence band. The bottom part of the conduction band is formed mainly by cerium ion empty states. Semi-localized 5d-Ce^{3+} states are delimited in the figure by a dashed line. The decay profiles recorded at various excitation energies are pictured in Fig.13.

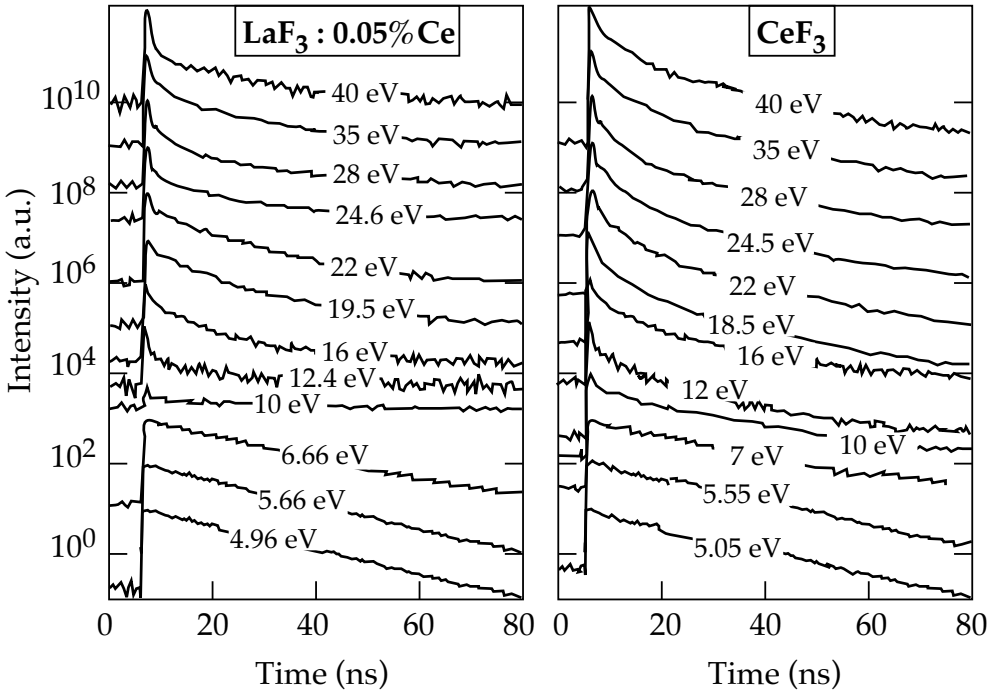

Fig. 13: 300 nm fluorescence decay profilesof LaF_3:0.05% Ce and CeF_3 obtained at room temperature under various excitation energies in the 0–80 ns time range

4.3.2 Interpretation of the mechanisms

From careful examination of experimental data, the dominant processes occurring at various excitation energies have been identified. Their description, given in detail in Ref.[31], can be summarized as follows:

– process 1 (4–6eV): intra-ion mechanism in Ce^{3+} ions
– process 2 (>6.5eV): ionization of Ce^{3+} ions
– process 3 (>9eV): creation and transfer of excitons
– process 4 (>12 eV): creation and transfer of electron-hole pairs
– process 5 (>16eV): excitation by a hot electron, electronic excitation multiplication
– process 6 (>20eV): core hole excitation by Auger relaxation

Processes 1 and 2 result in cerium fluorescence with a typical decay time of 20ns. These processes are included as final stages for all other processes (3–6). The latter processes can be subdivided into two groups: (a) energy transfer by relaxed electronic excitations, namely by excitons (process 3) and electron-hole pairs (4), and (b) energy transfer by hot electrons (5) and core holes (6). A luminescence excitation spectrum for photon energies ranging from 9 to 40eV displays intervals where one of these processes dominates and thus one can estimate its efficiency.

Photons with an energy close to the fundamental absorption edge (9–11.5eV) create mainly excitons which efficiently excite cerium luminescence (process 3). The peaks in the excitation spectrum and exponential fluorescence decay correspond to these energies. The increase of the kinetic energy of an electron-hole pair results in the decrease of the probability of exciton creation after thermalization since the thermalization length increases with particle kinetic energies. Therefore the excitation spectrum for photon energies above 12eV gives information about the cerium excitation efficiency by non-correlated electrons and holes.

Cerium ion excitation by photons with an energy between 12 and 16eV mainly arises through process 4. The excitation spectrum displays low efficiency of this process for CeF_3. Decay kinetics is characterized mainly by a slow component. The main reason is the energy position of the Ce 4f level at about 4–5eV above the valence band top [34,35], and thus the hole capture seems to have low probability since the 4f level is situated at rather too high an energy with respect to the top of the valence band. It should be mentioned that in Ref.[23] the process which was supposed to involve an electron capture followed by a hole capture is also not observed. Low efficiency of process 4 is one of the main limitations of the light yield of CeF_3, since the probability of creation of valence band holes after high-energy excitation is sufficiently high.

The fluorescence quantum yield increases when the electron kinetic energy in the conduction band is about 5–6eV [30,31,36] (Fig.12). Such an electron can excite a Ce 4f electron through an inelastic impact process [36]. There is no strong decrease of the excitation efficiency above the inelastic processes (5, 6) threshold [30,31]. Some oscillations can be explained by the variation of the energy distribution of secondary electrons depending on the type and energy of primary electronic excitations. The energy yield of CeF_3 fluorescence becomes constant for X-ray excitations [33].

This excitation spectrum analysis allows us to conclude [31] that direct excitation of Ce^{3+} ions (either by photons or by impact process) is the most effective way for the energy transfer to the cerium subsystem. The impact excitation probability can be estimated when the density of different states is taken into account. The highest lying filled states in CeF_3 are formed by one Ce^{3+} 4f electron and by eight F^- 2p electrons. Therefore, the energy transfer in the inelastic scattering process of a high-energy electron results in the excitation of the fluorine subsystem with a probability of around 90–95% and the cerium subsystem with probability of around 5–10%. These probabilities change for electrons that have a relatively low kinetic energy (5–9eV). Such electrons can excite only Ce^{3+} ions. The excitation of these ions is possible during the core hole relaxation as well, but most core holes produce excitation of the fluorine subsystem. The estimation based on the above-mentioned picture of the excitation process gives a mean energy for the production of one cerium excitation of 80–150eV [37]. This results in 7000–12000photons per MeV, which is 3–4 times larger than the experimental value.

The light yield overestimation is based on the account for all excitation processes and on the supposition that all excited cerium ions emit fluorescent photons. The quenching of a part of Ce^{3+} excited ions reduces this estimation. The process, which reduces the scintillation efficiency, is the joint relaxation of the excited Ce^{3+} with a neighbouring one or another electronic excitation [24,29]. This effect is observed only for photons with an energy above 18eV, which is the threshold for electron excitation multiplication. The fluorescence decay rate for initial decay stages after this excitation is much faster than the radiation time (20ns) (Fig.13) [31]. This effect depends on the initial spatial distribution of excited cerium ions, i.e. on the excitation photon energy. The quenching increases near the core level transitions threshold, when the relaxation of a core hole results in the production of several electronic excitations surrounding the initially excited ion [31]. This spatial distribution is not at equilibrium and the effect depends on the rate of spatial relaxation. When the temperature

increases, the migration rate of excitations over the cerium subsystem increases and therefore the quenching mechanism decreases [24]. It is difficult to estimate directly this quenching since the spatial distribution is unknown but the quenching factor can be estimated by the comparison between the area under the experimental decay curve and the single exponential curve with Ce^{3+} radiation time [25]. This comparison gives an additional reduction factor of about 0.2–0.5. The estimate of the light yield taking into account this additional reduction factor is in good agreement with experimental estimates.

4.3.3 Conclusion on the discussion

The discussion of the cerium excitation processes results in the following recommendations to increase the light yield:

(1) increase the probability of the valent hole capture (process 4),
(2) increase the fraction of excitons or electron-hole pairs (process 3),
(3) decrease the quenching due to interactions of excited ions.

Obviously the phosphorescence will be decreased in cases (1) and (2). At present, there is no final recipe on how to carry out these recommendations. Recently, investigations of $La_{(x)}Ce_{(1-x)}F_3$ solid solutions [38] and PrF_3-Ce [39] were made. In solid solutions with x = 20–80%, an increase of the fluorescence light yield and a simultaneous decrease of the phosphorescence are observed. This can be explained by an increase of process 3 in the energy transfer. The Pr 4f level is much closer to the valence band than that for Ce. Therefore the valent hole capture is easier and process 4 is more important in the fluorescence excitation. The probability of the energy transfer from Pr to Ce ions is high since the corresponding emission and absorption spectra are well overlapped. It can be expected that the scintillator based on the solid solution of PrF_3 and CeF_3 will have all CeF_3 advantages and will have high fluorescence light yield and low phosphorescence.

5. RADIATION DAMAGE

The very high particle flux at the new generation of high-energy colliders imposes severe constraints in the radiation resistance of the detector components. Thus, intensive studies of the radiation damage in CeF_3 with different sources of gammas, neutrons, or electrons at different dose rates were performed.

5.1 Gamma irradiation at room temperature

5.1.1 Generalities

The usual procedure for studying the CeF_3 crystals' behaviour under gamma irradiation was to measure the optical transmission of the sample before and after irradiation and calculate the induced absorption coefficient (see definition in Section3.1). Usually, the first measurement took place less than one hour after irradiation.

After a specific treatment on the purity of the raw material, particularly a reduction of oxygen contamination, some crystals grown by different producers with different raw materials present no radiation damage (Fig.14) [16,17,26]. For crystals presenting some damage, two different behaviours are observed. For some crystals, generally grown with bad quality raw material, a pink coloration appears after irradiation, due to the presence of two absorption bands at 320nm and at 500nm (Fig.15a) (first behaviour). For other crystals, grown with standard

quality raw material or doped with a divalent cation, two strong UV absorption bands at 340nm and 385nm appear, with in some cases two additional weak bands at about 450nm and 550nm (Fig.15b) (second behaviour). These two behaviours may be observed in some cases on the same crystal, the second one at the seed part and the first one at the other side.

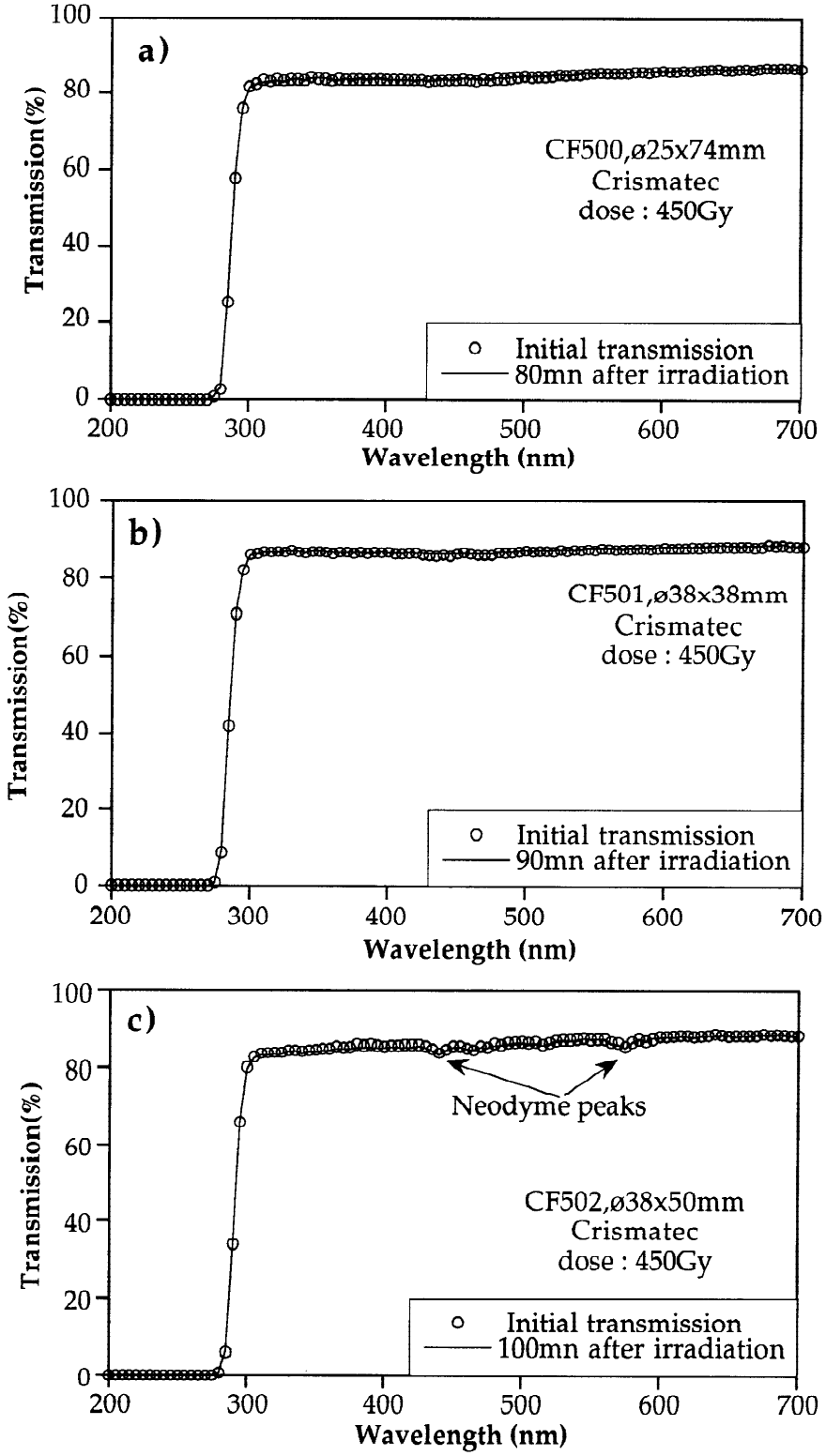

Fig. 14: Effects of radiations on several crystals (from Crismatec) after 500 Gy irradiation ^{60}Co

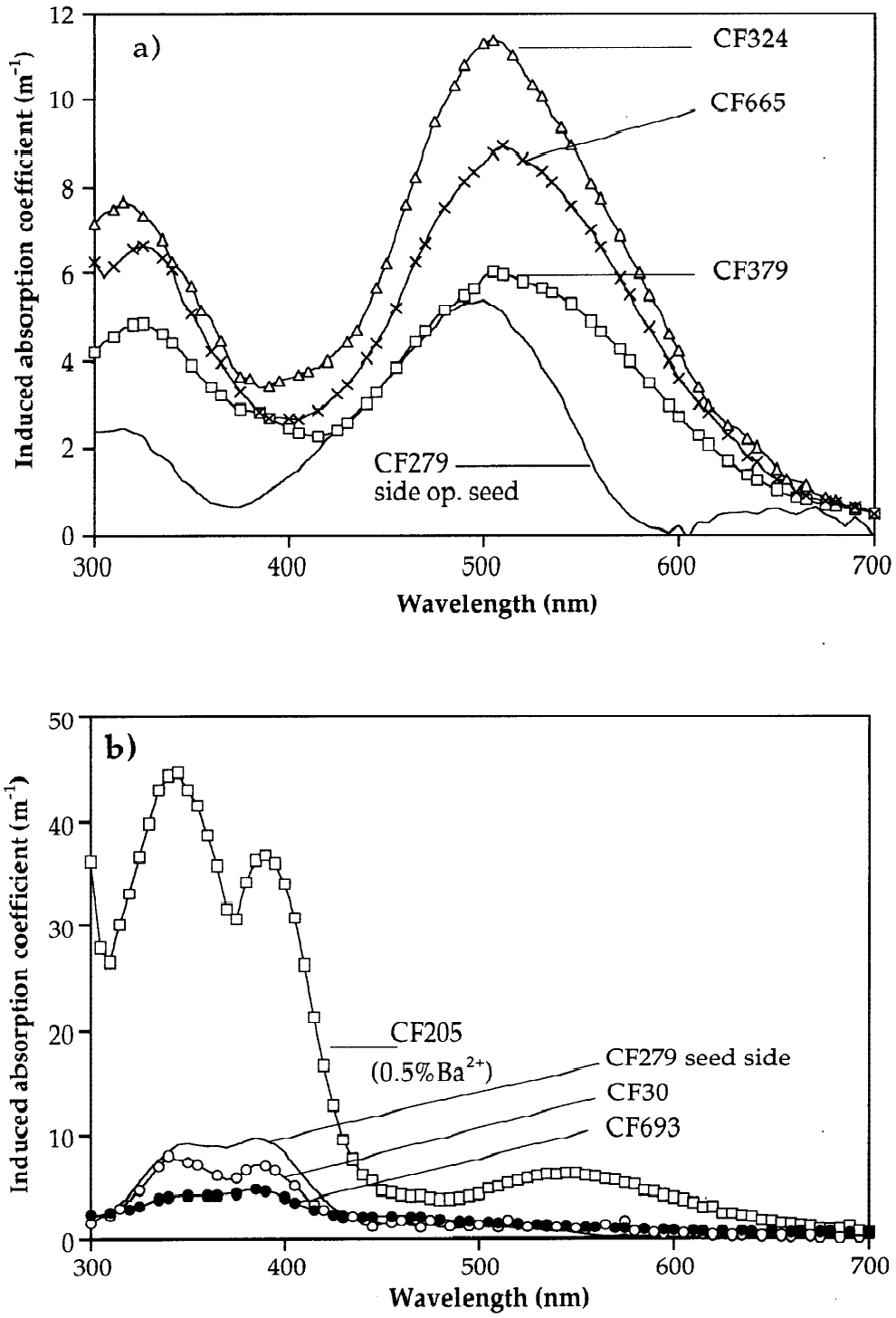

Fig. 15: Different behaviours of CeF_3 crystals under gamma irradiation: a) first behaviour in the text; b)second behaviour in the text

For long crystals, in the case of a dispersion of the optical absorption edges measured transversally along the growth axis, a strong gradient of the damage is observed. This effect, higher at the side opposite to the seed, reflects the segregation of the impurities which occurs during the growth process. For a new generation of long crystals, with no dispersion of optical absorption edge, the damage is null or low and no gradient is observed.

5.1.2 Recovery

In order to characterize the different defects associated with the various induced absorption bands, the damage recovery has been studied at room temperature and by thermal and optical treatment [16].

5.1.2.1 Recovery at room temperature

The recovery at room temperature was systematically studied on all the irradiated crystals during a period lasting from one week to several months [16].

For crystals showing the first behaviour, a continuous recovery is observed in the first week after irradiation and the remaining absorption coefficient is low (Fig.16) or even null. The evolution of the absorption coefficient at the maximum of the two absorption bands as a function of time after irradiation reveals the existence of several recovery regimes for the two bands (Fig.16). The kinetic of the recovery can be described by a sum of two exponentials (time constants around 10h and 50h) and a constant term (residual damage).

For the crystals showing the second behaviour, the recovery from the damage depends on the quality of raw material used for the crystal growth and on the doping. For most of the undoped crystals which present this behaviour, a fast recovery is observed in the first three hours, but a stable damage remains (Fig.17a). For the recent crystals grown with 'highly purified' raw material, a strong and fast recovery is observed during the first day after irradiation and a low residual damage remains (Fig.17b). A similar recovery is observed on barium-doped crystals (Fig.17c).

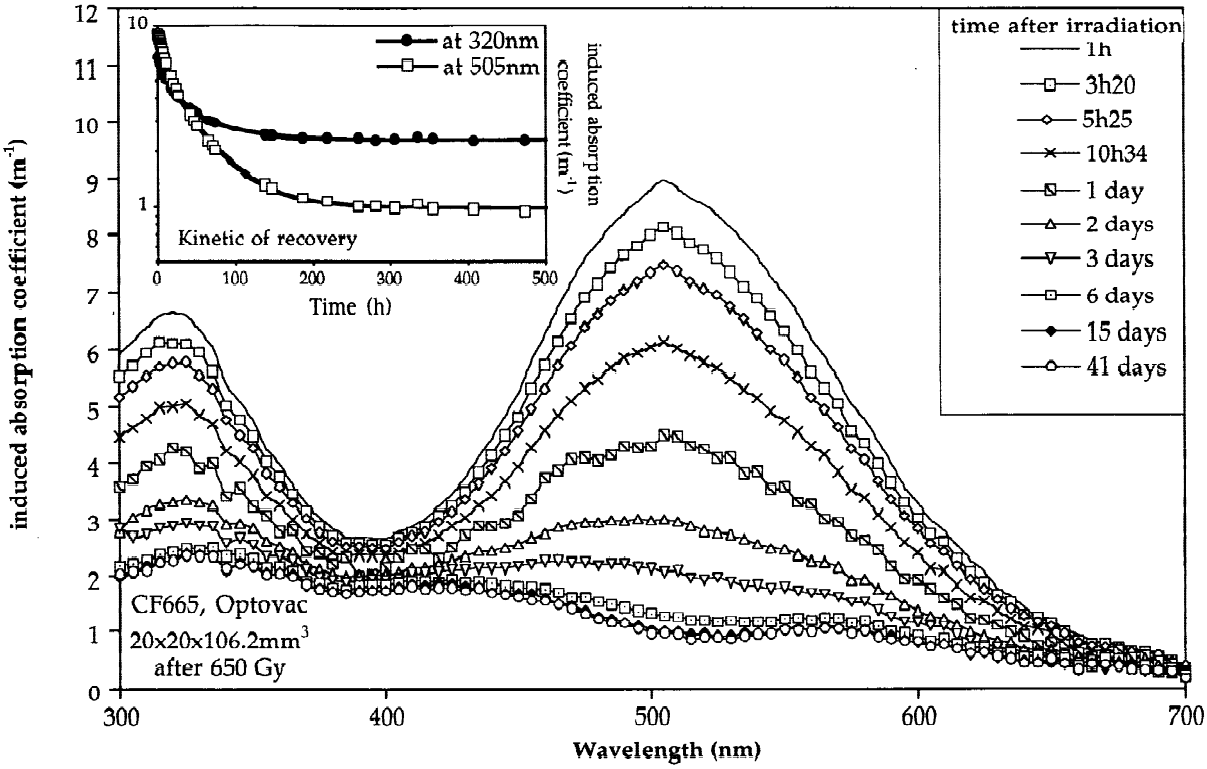

Fig. 16: Recovery at room temperature of a crystal (CF665 from Optovac, after 650 Gy) presenting the first behaviour. Inset: recovery kinetics at induced absorption band maxima

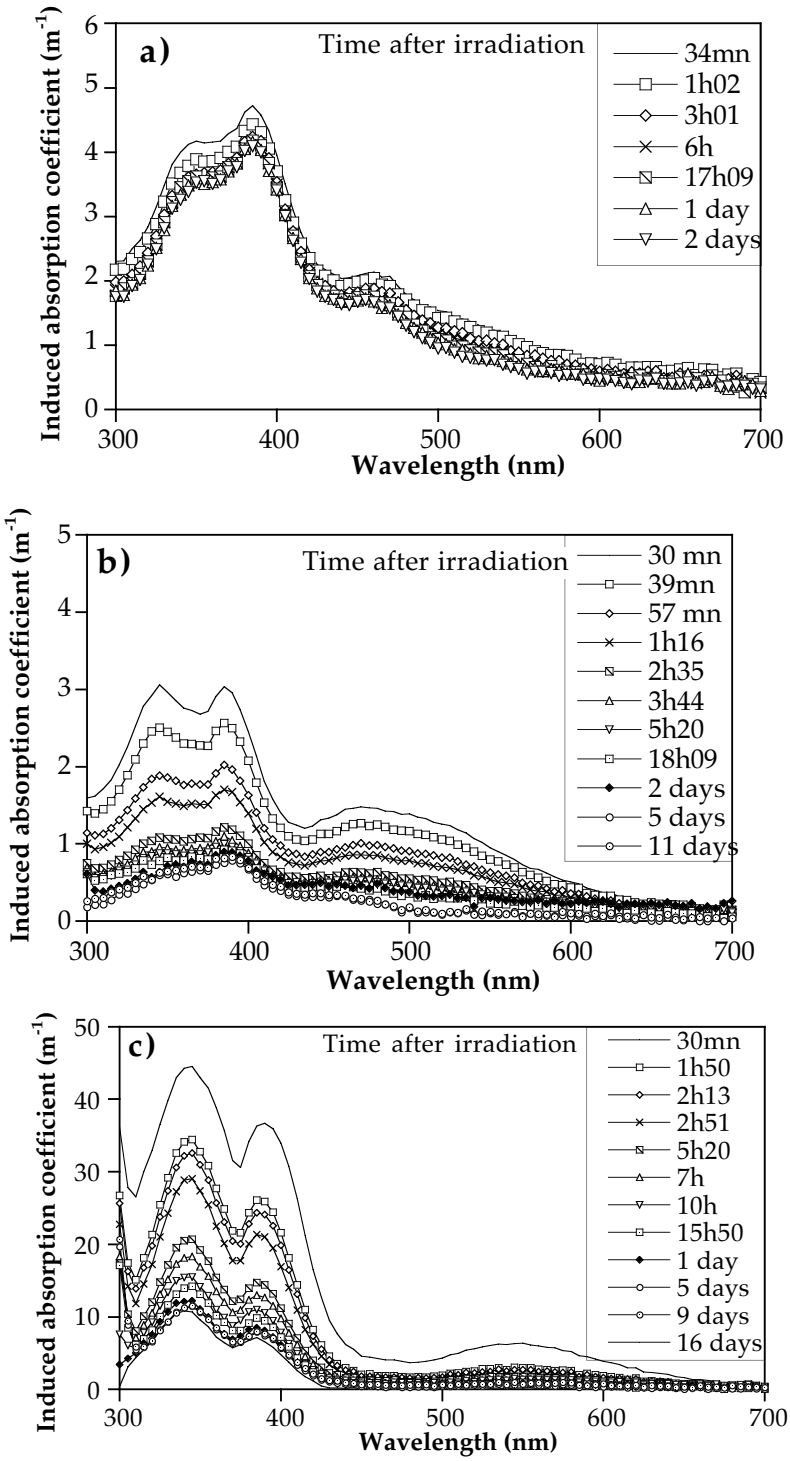

Fig. 17: Recovery at room temperature of crystals presenting the second behaviour: a) first received crystal (CF693 from MKT, after 660 Gy); b) recently received crystal (CF552 from Optovac, after 640 Gy); c)barium-doped crystal (CF205 from Optovac, after 300 Gy)

The evolution of the absorption coefficient at the maximum of the absorption bands as a function of time after irradiation can be approximated by a sum of two exponentials and a constant term. However, the time constant of the two exponentials and the constant term vary from crystal to crystal. Typical values are summarized in Table 3 (μ_i is the value of induced absorption measured just after irradiation).

Table 3

Recovery parameters for the second behaviour

Crystal	Band	Fast recovery time constant (h)	Slow recovery time constant (h)	Residual absorption (% μ_i)
'Old' undoped	340 & 385 nm	0.6	29	~ 80
	500 nm	1	16	~ 80
Barium-doped	340 & 385 nm	3	20	< 20
	500 nm	1	14	~ 80
'New' undoped	340 & 385 nm	0.5	6	< 20
	500 nm	6	10	< 20

5.1.2.2 Recovery with temperature

A thermal treatment was applied to those crystals which still had a residual damage several weeks after irradiation. The crystals are gradually heated up to 300°C in steps of about 50°C in a vacuum furnace (10^{-5}torr) for six hours. After each step, their optical transmission is measured immediately after cooling. It is possible to heat the crystals above 300°C, but in this case, a black coloration located in the first 1 or 2mm from the crystal surface is observed, accompanied by a new induced absorption band at 320nm [17]. This effect is attributed to crystal oxidation [17].

In the case of the first behaviour, a partial recovery is observed after a 100°C annealing. A total damage recovery is possible for the two bands after heating at 150°C [16].

For the second behaviour, no effect is visible up to a temperature of 250°C. Then, a sizeable recovery is observed at 300°C, but a residual damage remains even after 24h of thermal treatment at 300°C, except for the barium-doped crystals [16].

5.1.2.3 Optical bleaching

We have tried to anneal the residual damage observed in some crystals by means of exposure to light. A 50mW argon laser (514nm) does not produce any effect even after several hours. UV lamps (mercury and xenon) were then tested. Only with 150W xenon light, filtered out below 300nm to limit the creation of free carriers by exciting the crystal at too high an energy, and focused on the crystal, a very small effect is observed in the first two hours for all crystals [16,17].

5.1.3 Saturation with the dose

Several crystals were irradiated with doses increasing in steps in order to study a possible damage saturation. The shape of the absorption spectra remains constant, but the intensity of induced absorption increases (Fig.18). For small doses, the intensity increases linearly; but for all the crystals, whatever the behaviour, a saturation progressively occurs. However, the saturation is reached at different doses for each crystal. For instance, for doped crystals, the saturation is reached for a dose of 35kGy [17,40], while for undoped crystals, it is reached after less than 2kGy. In the latter case, if purer raw material is used for the growth of crystals, the saturation dose is lower [16].

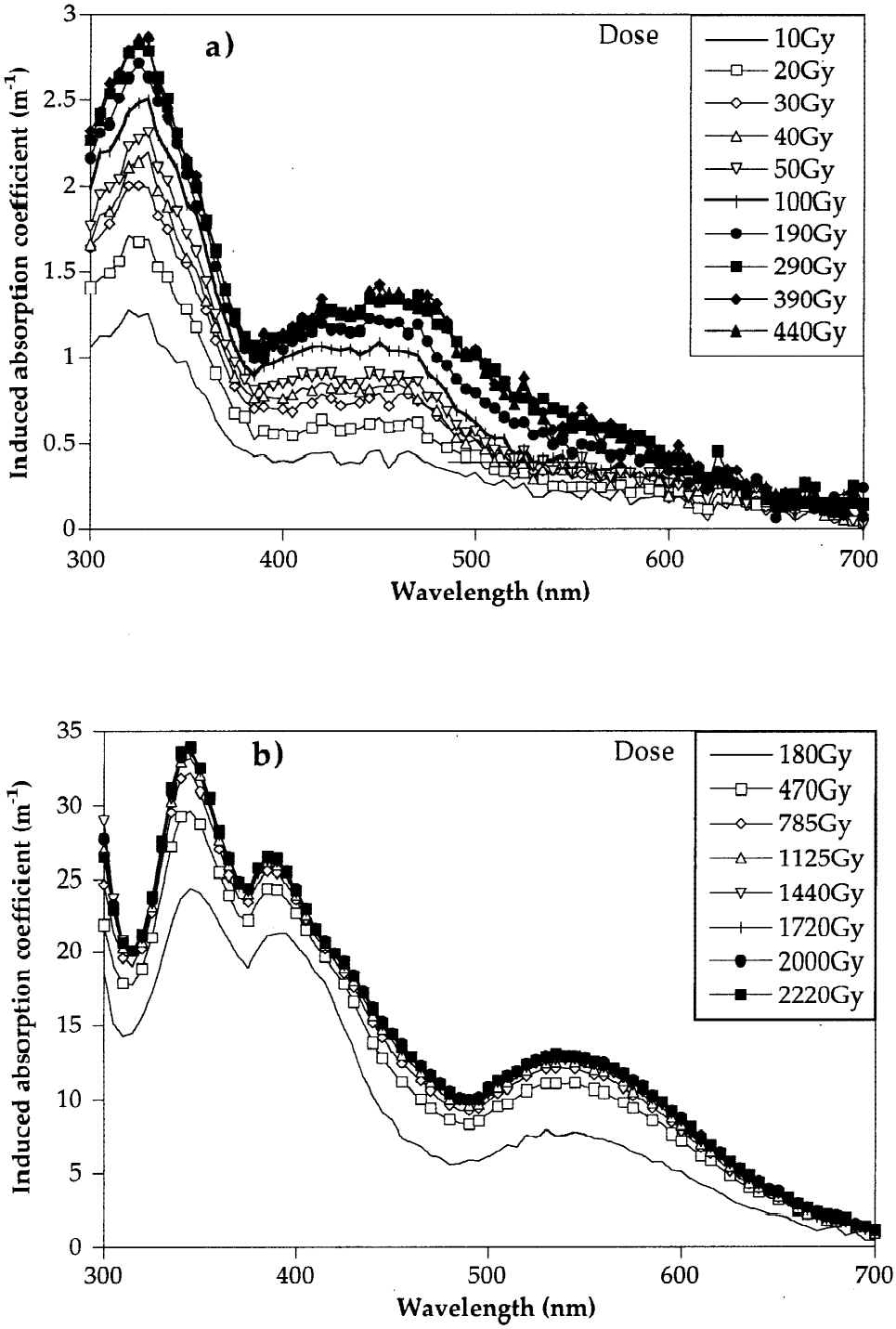

Fig. 18: Saturation of the induced damage for two crystals: a) presenting the first behaviour (CF645 from Optovac); b) presenting the second behaviour (CF391 from NKK)

5.1.4 Thermoluminescence

Thermoluminescence measurements were made on several crystals presenting the two different behaviours under irradiations. For all of the crystals, the signal is either non-existent or very weak [16,17]. These results are confirmed by other groups [27,40]. The fact that recovery at room or higher temperatures is observed and that the thermoluminescence signal is absent leads to the conclusion that damage recovery is essentially non-radiative.

5.1.5 Polarization of the damage

The measurements of the absorption spectra with linearly polarized light on oriented crystals show that the radiation damage is strongly polarized [16,26,41]. For the second behaviour, the absorption bands are stronger when the polarization is parallel to the *c*-axis, this is also observed for the absorption at 500nm of the first behaviour, but at 320nm the absorption is stronger for polarization perpendicular to the *c*-axis. The high polarization of this damage suggests that they are oriented in preferential directions in the lattice. The radiation effects in CeF_3 are probably related to the presence of fluorine vacancies. In the CeF_3 structure (tysonite), three types of fluorine sites exist with different cerium coordinations [42]. The mobility of one of these fluorine ions is higher, creating a preferential site for fluorine vacancies.

5.1.6 Irradiation at low temperature

Low-temperature irradiation was performed in order to obtain information about the primary defects created in the crystal by energetic radiation [12]. For most of the crystals, two large absorption bands appear at 475nm and 700nm after an irradiation at 80K. Up to room temperature, three steps in the annealing can be observed [12]: The intensity of the two large bands decreases from 80K to 100K. The structure of the absorption spectrum is modified in the range from 100K to 200K, where the two previous bands disappear, while two new bands appear in the UV region. Above 200K, the absorption spectrum is stable and only the intensity of the UV bands decreases. They are similar to the ones observed after irradiation at room temperature (two UV bands at 340nm and 385nm). The same experiment has also been carried out by other groups [43,44]. A correlation of the absorption spectra modifications with the electronic paramagnetic resonance (EPR) measurements was performed. The EPR measurements confirm the creation of F centres at low temperature that are unstable at room temperature.

5.1.7 Discussion on radiation damage

The recovery, spontaneous or induced by optical and thermal bleaching, shows that the two kinds of damage observed on CeF_3 are certainly associated with different defects. For the first behaviour, the total recovery can be reached, while for the second behaviour, even with temperature, a stable damage remains. Moreover, the measurements of the absorption spectra with linear polarized light on oriented crystals confirm the different nature of the defects associated with the two kinds of damage.

In CeF_3 the most probable point defect is the fluorine vacancy which can trap an electron to form an F centre. In some cases, this defect can be associated with impurities present in the crystal, forming perturbed F centres which are generally more stable than solitary F centres. The influence of fluorine vacancies, and therefore of F centres, on the radiation damage was proven by irradiating crystals doped with divalent cations. The irradiation of barium-doped crystals shows [17] that the damage is higher than for undoped crystals. The divalent cation doping increases the number of fluorine vacancies (for charge compensation of cation impurities), and therefore the number of F centres.

This result, associated with EPR [43,44] and low-temperature [12] studies which show that F centres are an intermediate state of room-temperature radiation-induced defects, leads to the conclusion that F centres in combination with impurities play a major role in the radiation hardness of CeF_3.

The strong dependence of the intensity of the damage and of the saturation dose for both behaviours on the impurities present in the raw materials makes us conclude that the impurities play an important role in radiation hardness of CeF_3. This is confirmed by the fact that after an improvement of the raw material purity, particularly a reduction of the oxygen contamination, several crystals grown from different raw materials present no radiation effect after a strong gamma irradiation. Moreover, the fact that the two kinds of damage can be observed in the same crystal, the first one at the side opposite to the seed and the second one at the seed side, leads one to assume that these damages are associated with different impurities having different segregation coefficients.

From all these considerations, one can conclude that defects created by irradiation of CeF_3 are not solitary F centres, as was first supposed, but perturbed F centres.

5.2 Irradiation in an LHC-like environment

The main motivation for the study of CeF_3 is to prove its ability to match the requirements imposed on scintillating materials for high-rate electromagnetic calorimeters. Therefore, CeF_3 has been studied under LHC-like radiation conditions for gammas as well as for neutrons by different groups of the collaboration [11,13,14,17,45].

5.2.1 Damage for low γ dose rate

Two pure crystals (CF128, CF638) have been irradiated with increasing doses at an average rate of 1.2Gy/h, similar to the expected dose rate at the LHC for a pseudorapidity $|\eta| \sim 2$, at about 4m from the interaction region. The total accumulated dose was 5.3 ± 1.1 kGy [11,14,17] and 4.3kGy [45], respectively. The transmission measurement at the end of each irradiation period was compared to the transmission before irradiation. Both these crystals have been irradiated before with high dose rate (3Gy/min).

For the first one, which presented no effect after an irradiation of 1000Gy with the ^{60}Co source at the Geneva Cantonal Hospital, no damage was observed [17]. For the second one, which presented a small damage with a fast recovery after an irradiation of 500Gy, a slight effect has been observed after a low dose rate irradiation. After 4.3kGy, the absorption coefficient was below $0.2 m^{-1}$ [45].

5.2.2 Neutron-induced damage

As irradiations with reactor neutrons are usually contaminated by gamma rays, the crystals chosen for neutron irradiation, were first irradiated by gammas (100Gy), in order to be able to separate the gamma from the neutron contribution.

Four crystals (CF04, CF05 CF631, CF128) have been irradiated by MeV neutrons, the first three in Bombay [13,17], the last one in Saclay [14,17]. The irradiation was done in steps up to a total fluence of $1.9 \times 10^{13} cm^{-2}$ in Bombay and up to $10^{14} cm^{-2}$ in Saclay. Their characteristics are summarized in Table 4.

Table 4

Characteristics of crystals irradiated by neutrons

Crystal	Dimensions (mm)	Producer	γ irradiation effect
CF04	$10 \times 10 \times 10$	Optovac	visible effect (100Gy)
CF05	$10 \times 10 \times 10$	Optovac	no visible effect
CF631	$16 \times 16.7 \times 17.3$	Crismatec	no visible effect
CF128	$18 \times 17 \times 9$	Optovac	no visible effect

The optical transmission of the four crystals at two different wavelengths (320nm, 360nm) is plotted in Figs.19a and 19b as a function of the integrated neutron fluence. The three crystals (CF05, CF631, CF128), which were resistant to gamma rays, do not show any appreciable loss of transmission up to a fluence of about 10^{13}n/cm^2. For the crystal CF04 which was less resistant to gamma rays, the transmission drops from 80% to about 60% in the UV region ($\lambda \leq 400$nm) for a fluence of 10^{12} neutrons. This crystal shows a similar drop in transmission after a gamma irradiation of 100Gy, which is the residual gamma flux expected in the neutron irradiation chamber behind the lead shield. The effect observed on that crystal can thus be attributed to the gammas and not to the neutrons. It is not the case for the effect observed on CF128 after 10^{14} neutrons, since this crystal is strongly radiation-hard to gammas [17]. This effect has been attributed to fast neutrons [14].

We can therefore conclude that cerium fluoride crystals, even of rather poor quality (CF04), are radiation-hard to fast neutron irradiation up to a fluence of 5×10^{13}n/cm^2 which is slightly higher than the maximum annual dose foreseen at the LHC.

The CeF_3 induced radioactivity was measured after irradiation. The gamma activity was always at the background level (0.1mrem/h). The β activity has been measured to be 0.07mrem/h after an irradiation of 5×10^{12}cm^{-2} neutrons in the MeV region, dying out with a typical lifetime of 12hours.

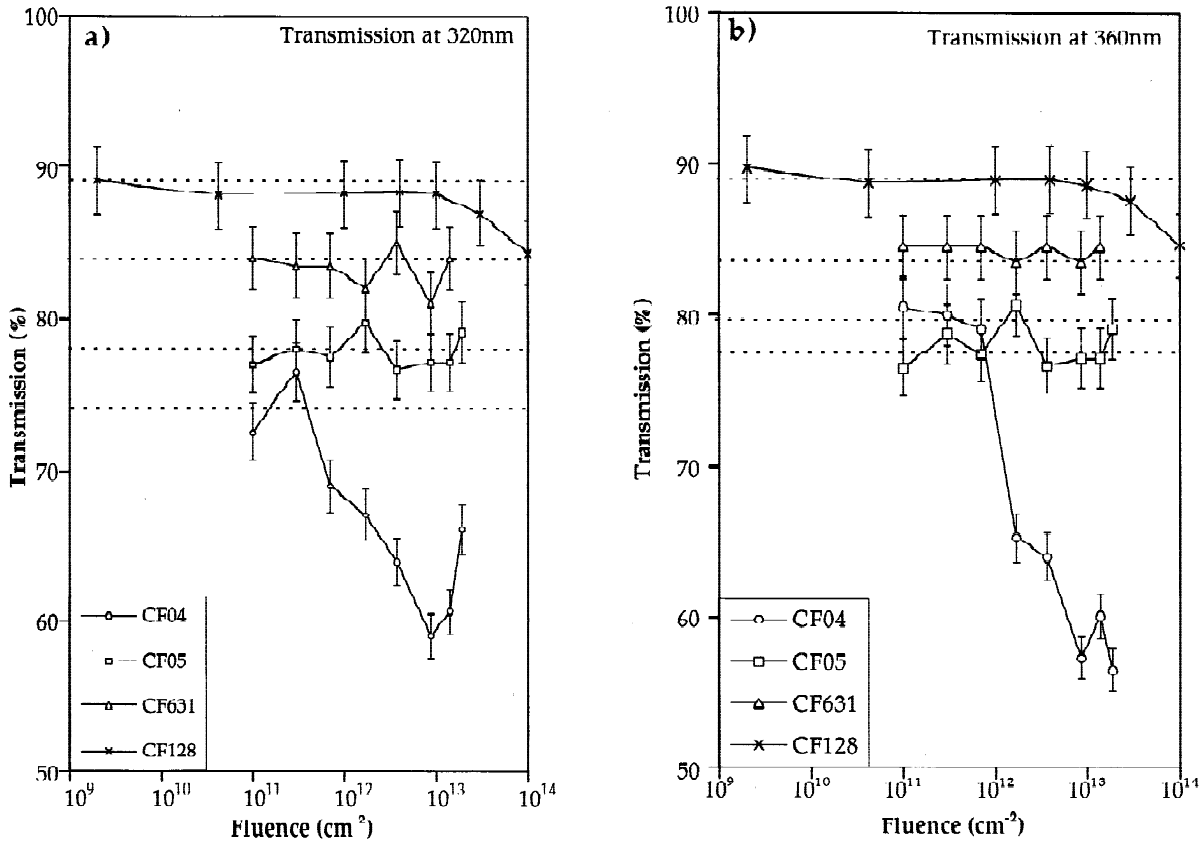

Fig. 19: Evolution of the optical transmission after neutron irradiation: a) at 320 nm; b) at 360 nm

6. BEAM TESTS

As far back as 1993, the Crystal Clear Collaboration tested several long CeF_3 crystals in a high-energy beam [46]. At the end of 1993, CCC and the Swiss Federal Institute of Technology, Zurich (ETHZ) started a collaboration to evaluate the feasibility of a cerium fluoride calorimeter for the CMS experiment [47]. Since 1991, ETHZ has a joint research agreement with the Shanghai Institute of Ceramics and with the Beijing Glass Research Institute to produce and test large CeF_3 crystals. The results presented here are based on data taken on a common crystal matrix between April and September 1994 in two CERN SPS test beams at momenta ranging from 10 to 150GeV/*c*. For more details and explanations, see Refs.[48] and [49].

6.1 Test set-up

A longitudinally segmented crystal matrix was built from the best available crystals. They had a cross-section of $3\times3\text{cm}^2$ except for the four corners that were $2\times2\,\text{cm}^2$. The total length of the towers was made as close as possible to $25\,X_0$ (42cm). The front segments consisted of single crystals with length near to 14cm, while the back segments typically consisted of two crystals glued together to obtain a length close to 28cm. Detailed dimensions of the crystals, light yield, and residual non-uniformity after uniformization of the light collection along the length of the crystals can be found in Table 5. The resulting crystal matrix was far from perfect from a geometry and quality viewpoint.

Table 5

Parameters of the CeF_3 matrix. Tower 5 is the central tower, while towers 1, 3, 7 and 9 are placed in the corners. The light yield and non-uniformity were measured in the laboratory with a photomultiplier and a ^{60}Co source

Tower	Segment	Dimensions (mm)	Total length of tower (mm)	Light yield (photons/MeV)	Non-uniformity (%)
1	Front	20×20×126		1082	4.2
	Back	20×20× (140+140)	406	490	4.9
2	Front	32×33×114		1040	2.5
	Back	30×30× (140+140)	394	380	12.2
3	Front	20×20×140		980	6.2
	Back	20×20× (100+167)	407	1013	4.6
4	Front	28×29×141		720	6.4
	Back	30×30× (80+80+100)	400	280	23.6
5	Front	30×30×148		550	8.3
(Central)	Back	30×30× (140+140)	428	650	6.6
6	Front	31×31×132		370	11.3
	Back	30×30× (140+140)	413	440	15.5
7	Front	21×21×140		846	9.7
	Back	20×20× (125+128)	393	459	–4.3
8	Front	28×28×141		700	9.7
	Back	29×29×255	396	400	6.6
9	Front	20×20×140		523	8.8
	Back	20×20× (140+106)	386	359	6.9

The light was collected by $1\times1\,\mathrm{cm}^2$ windowless Hamamatsu Silicon Photodiodes (SPD) at the extreme ends of each tower. The SPD signal was sent to a slow amplifier chain consisting of charge preamplifiers [50] and standard RC-CR shaping amplifiers [51] (shaping time ~2ms). Tests were also conducted on one tower with fast bipolar current amplifiers [52] (shaping time ~20ns). The crystal matrix was fitted in a double shielded box with remote position control.

Electron, pion and muon beams, with energies ranging between 10 and 150GeV, were used to test the matrix in the X3 and H4 beam lines at CERN.

6.2 Results

For calibration purposes, a pion beam was aimed at each of the towers. This gave rise to three peaks in the ADC spectrum (Fig.20):

- a Gaussian pedestal peak, the width of which is a measurement of the electronic noise;
- a Landau light peak, due to the minimum-ionizing pions depositing their energy by Bethe–Bloch ionization along the length of the crystal;
- a peak that is the convolution of the Landau light peak and a Landau peak generated by direct energy deposit of the pions in the depleted zone of the SPD.

Note that the pion interactions are out of the ADC scale.

Using the pion measurements, the noise for the best quality crystal was evaluated at 5MeV for slow and 12.4MeV for fast electronics.

Using the value of $\mathrm{d}E/\mathrm{d}x$ for a minimum-ionizing particle in each CeF_3 segment determined by Monte Carlo simulations and the number of electron-hole pairs liberated by such a particle in a 300mm thick silicon depleted layer [46], the two latter peaks allow the calibration of the ADC channels in energy and in photoelectrons. This results in light yield values (calibration factors) for each segment ranging between 20 and 200 photoelectrons per MeV. When a 50GeV electron beam is aimed at the centre of each tower, the observed anticorrelation between the energy deposited in the front and in the back segment allows an accurate front–back intercalibration for each tower. Monte Carlo simulations of the energy deposit in each crystal compared with the measured deposits provide another way of calibration of each crystal which was generally used for the tower summation.

By summing the energy deposits in the nine towers and fitting the resulting peak with a Gaussian, an energy resolution of ~0.5% is obtained for energies of 50GeV (Fig.21) and higher. The tail towards high energies contains about 10% of the events and is due to a direct deposit of energy (nuclear counter effect) in the photodiodes (front and back) by shower particles. These events lead also to a widening of the energy distribution, especially for higher electron energies for which the intrinsic resolution is smaller. Figure22 shows the excellent agreement of measurements with the Monte Carlo results. The Monte Carlo simulation was performed with and without the nuclear counter effect to show its contribution to the widening of the energy peak. The nuclear counter effect can be decreased by using longer crystals with higher light yield and photodiodes with a thinner depleted zone. It will probably disappear altogether when using low-gain avalanche photodiodes (which have a very small effective thickness of the depleted region).

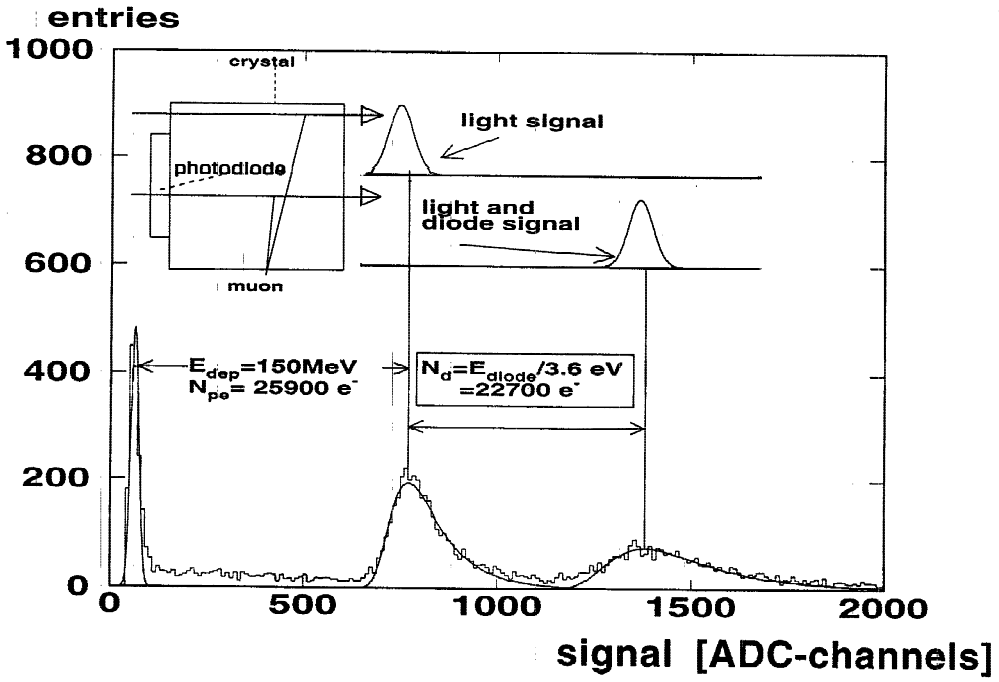

Fig. 20: Typical pulse-height distribution of non-interacting pions of 50 GeV in the front crystal of tower 1. The pion interactions are out of the ADC scale

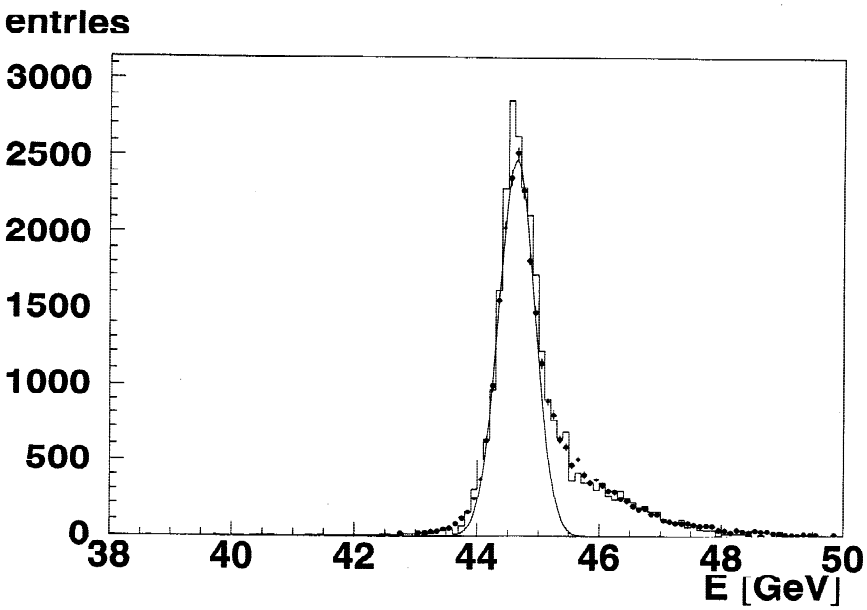

Fig. 21: Energy distribution of the full matrix for 50 GeV electrons (0.5% subtracted for momentum dispersion in X3 beam line [53]). The agreement between the measured points and the Monte Carlo simulated histogram, taking into account the nuclear counter effect in front and back SPD, is excellent

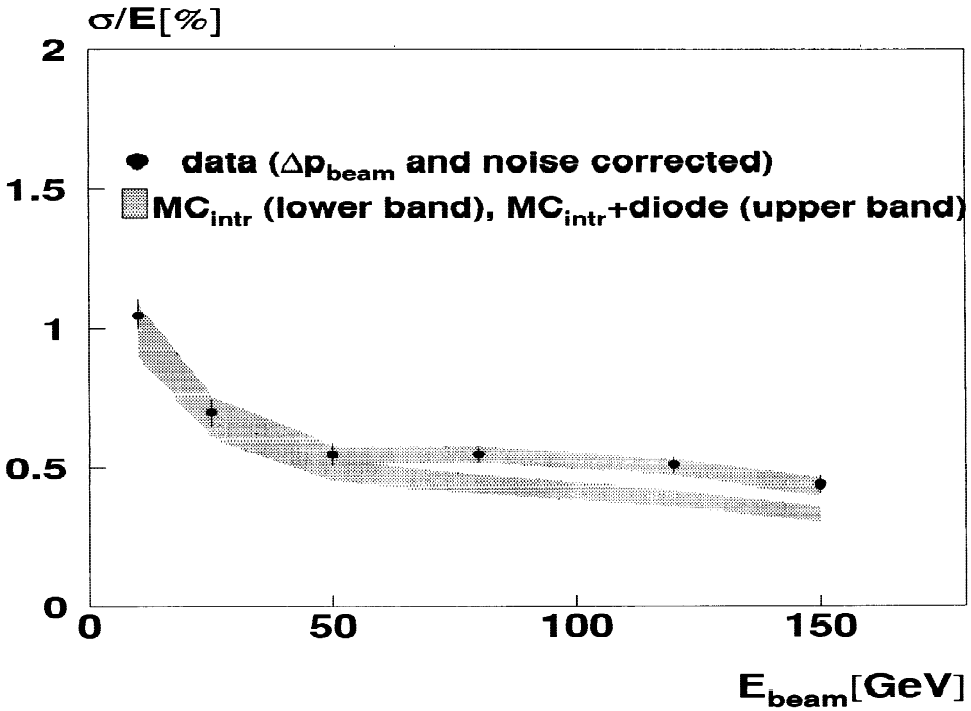

Fig. 22: Experimental results and Monte Carlo simulation comparison for electrons. Here again the agreement of data with Monte Carlo including the SPD effect is very good

Using the reconstructed barycentres in the front and back segments, position resolutions of respectively 0.8 and 1mm were obtained for 50GeV electrons. Using the whole shower yields a 0.7mm position resolution. The two barycentres and a 8.5cm lever arm result in an angular resolution of 15mrad for 50GeV electrons.

The hadron contamination at 50GeV is measured to be below 5% with a total energy cut and 0.15% when a cut on the front segment is added. Adding rejection by lateral dispersion analysis, a pion contamination well below 0.1% for an electron efficiency of about 99% is obtained.

In conclusion, energy resolutions of around 0.5% for electron momenta ≥ 50GeV have been reached for a non-optimal, segmented CeF_3 matrix. The experiments showed no problems with electronic noise. The measured energy resolutions over the range 10–150GeV indicate the excellent adequacy of the crystal as a Higgs hunting tool in the 2-photon decay sector [54,55]. The high-energy tail observed can be reduced by using longer, high-quality crystals, and/or avalanche photodiodes for the readout. The fine granularity allows the determination of the position with a resolution of ~0.7mm for 50GeV electrons. Longitudinal segmentation allows reconstruction of the photon angle with a precision of 15mrad and improves the electron/hadron discrimination significantly.

7. CONCLUSION

After extensive studies on CeF_3 scintillation and radiation resistance mechanisms, the Crystal Clear Collaboration established that this crystal is well suited for high-energy calorimetry. Several good features such as fast response without afterglow and potentially good resistance to radiation are confirmed as well as its excellent behaviour in a high-energy electron beam. The possibility of growing long crystals of high quality was assessed.

For the CMS calorimeter project at the LHC, which was examined by physics committees against a background of budgetary restrictions, CeF_3, despite its good performance, appeared to be an expensive solution, even if a target price of \$2/cm^3 could be achieved. In the mean time, another crystal, the lead tungstate ($PbWO_4$) was developed [56,57] and produced. Its very high density (8.3g/cm^3), reducing the necessary volume by a factor of ~2, and the relatively easy production conditions should reduce the cost of the crystals for a calorimeter by more than a factor of 2 with respect to CeF_3. Moreover, the recent development of Avalanche Photodiodes (APDs) make it possible to use the relatively scarce light produced by $PbWO_4$ without significant decrease of the calorimeter performance. In October 1994, the CMS Collaboration decided to take crystals as a baseline for its calorimeter and proposed $PbWO_4$ as the first choice.

To be able to use CeF_3 in a large calorimeter at a high-rate machine, more R&D with the producers would be required in order to optimize the production conditions for the particular crystal characteristics and desired geometry and to define realistic economic conditions. The intrinsic qualities of CeF_3will certainly yield diverse applications for this crystal even outside the high-energy physics field, in particular when not too large crystal dimensions and volumes are required, such as for astrophysics and medical imaging detectors.

Acknowledgements

The authors wish to express their gratitude to the teams of the companies Crismatec (France), Monokrystaly Turnov (Czech Republic), NKK (Japan), Optovac (USA), Shanghai Institute of Ceramics and Beijing Glass Research Institute (China), and Vavilov State Optics Institute (Russia) for the crystal procurement and fruitful cooperation. We would also like to thank all the members of the Crystal Clear Collaboration and the ETH Zurich and IPN Lyon staff members who were deeply involved in the beam tests.

References

[1] The Crystal Clear Collaboration, R&D Proposal for the Study of New Fast and Fadiation Hard Scintillators for Calorimetry at LHC, CERN/DRDC P27/91–15 (1991).

[2] D.F. Anderson, IEEE Trans. Nucl. Sci. **36** (1989) 137.

[3] W.W. Moses and S.E. Derenzo, Nucl. Instrum. Methods Phys. Res. **A299** (1990) 51.

[4] I. Oftedal, Z. Physik. Chem. **B13** (1931) 190.

[5] A. Zalkin, D.H. Templeton and T.E. Hopkins, Inorg. Chem. **5** (1966) 1466.

[6] C. Laviron and P. Lecoq, internal report, CERN–PPE.

[7] M. Nikl et al., J. Lumin. **60**&**61** (1994) 971.

[8] C. Pédrini, B. Moine, J.C. Gacon and B. Jacquier, J. Phys. Cond. Matter **4** (1992) 5461.

[9] L.M. Bollinger and G.E. Thomas, Rev. Sci. Instrum. **32** (1961) 1044.

[10] Millipore, Filter paper 0.45μm HAWP00010, Millipore SA, St Quentin, France.

[11] R. Chipaux et al., Nucl. Instrum. Methods Phys. Res. **A345** (1994) 440.

[12] E. Apostol et al., to be published in Radiation Effects and Defects in Solids, **133–134** (1995).

[13] S. Banerjee, S. Mangla, G. Mazumdar and R. Raghavan, TIFR/EHEP/94–12(1994).

[14] R. Chipaux et al., Materials Research Society Symposium Proceedings, **348** (1994) 481.

[15] F.A. Jenkins and H.E. White, Fundamentals of Optics, (McGraw-Hill, New York, 1950).

[16] E. Auffray, Thèse de doctorat de l'Université Paris VI, 1995.

[17] The Crystal Clear Collaboration, S. Anderson et al., Nucl. Instrum. Methods Phys. Res. **A332** (1993) 373.

[18] G. Blasse and A. Bril, J. Chem. Phys. **51** (1969) 3252.

[19] F.A. Kroeger and J. Bakker, Physica, VIII n°7 (1941) 629.

[20] C. Pédrini, B. Moine, D. Boutet and P. Martin, Heavy Scintillators for Scientific and Industrial Applications, edited by F.DeNotaristefani, P.Lecoq and M.Schneegans (Editions Frontières, Gif-sur-Yvette, 1993), p.187.

[21] M. Nikl et al., Solid State Commun. **87** (1993) 185.

[22] M. Nikl and C. Pédrini, Solid State Commun. **90** (1994) 155.

[23] A.J. Wojtowicz, M. Balcerrzyck, E. Berman and A. Lempicki, Phys. Rev. **B49** (1994) 14880.

[24] C. Pédrini et al., Chem. Phys. Lett. **206** (1993) 470.

[25] M. Nikl et al., J. Phys. Condens. Matter, **7** (1995) 6355.

[26] E. Auffray, I. Dafinei, P. Lecoq and M. Schneegans, Materials Research Society Symposium Proceedings, **348** (1994) 111.

[27] A.J. Wojtowicz et al., Materials Research Society Symposium Proceedings, **348** (1994) 455.

[28] A.J. Wojtowicz, E. Berman, Cz. Koepke and A. Limpicki, IEEE Trans. Nucl. Sci. **39** (1992) 494.

[29] A.N. Belsky et al., Abstract book of the 10th International Conference on Vacuum Ultraviolet Radiation Physics, Abs. Tu26, Paris, (1992).

[30] W.W. Moses et al., J. Lumin. **59** (1994) 89.

[31] C. Pédrini et al., Materials Research Society Symposium Proceedings, **348** (1994) 225.

[32] A.N. Belsky et al., to be published.

[33] A.N. Belsky et al., to be published in Nucl. Instrum. Methods Phys. Res. (1995).

[34] K.H. Park and S.J. Oh, Phys. Rev. **B48** (1993) 14833.

[35] D. Bouttet et al., Int. Conf. on Inorganic Scintillators and their Applications, Delft, The Netherlands, August 28–Sept. 1, 1995.

[36] Yu. M. Aleksandrov, V.N. Makhov and M.N. Yakimenko, Sov. Phys. - Solid State (USA) **29** (1987) 1092.

[37] R.A. Glukhov and A.N. Vasil'ev, to be published in Radiation Effects and Defects in Solids, **133–134** (1995).

[38] A.N. Belsky et al., Int. Conf. on Inorganic Scintillators and their Applications, Delft, The Netherlands, August 28–Sept. 1, 1995.

[39] C. Pédrini et al., to be published.

[40] C.L. Woody, J.A. Kierstead, P.W. Leavy and S.P. Stoll, IEEE Trans. Nucl. Sci. **41** (1994) 675.

[41] E. Auffray, I. Dafinei, P. Lecoq and M. Schneegans, Radiat. Eff. Defects Solids **135** (1995) 337.

[42] Gmelin, Handbuch der anorganischen Chemie, Teil 39, Verlag Chemie GmbH Weinheim, Bergstrasse (1973).

[43] L.E. Halliburton and G.J. Edwards, Materials Research Society Symposium Proceedings, **348** (1994) 423.

[44] R.T. Williams, *in* Proc. Int. Workshop 'Physical Processes in Fast Scintillators', StPetersburg, Russia, 1994, edited by P.A. Rodnyi and C.W.E. Van Eijk.

[45] R. Chipaux and O. Toson, Int. Conf. on Inorganic Scintillators and their Applications, Delft, The Netherlands, August 28–Sept. 1, 1995.

[46] E. Auffray et al., Materials Research Society Symposium Proceedings, **348** (1994) 117; Preprint CERN-PPE/94–112.

[47] E. Auffray et al., Proc. Int. Conf. on Advanced Technology and Particle Physics, Como, Italy, 3–7 October 1994, Eds. E. Borchi, S. Majewski, J. Huston, A. Penzo and P.G. Rancoita, Nucl. Phys. B (Proc. Suppl.) **44** (1995) pp. 57–62. CMS Technical Note 94–271.

[48] E. Auffray et al., submitted to Nucl. Instrum. Methods Phys. Res., Preprint CERN-PPE/95–176.

[49] H. Hillemanns, Thesis, Aachen University, Germany, 1995.

[50] M. Goyot, Nucl. Instrum. Methods Phys. Res. **A263** (1988) 180.

[51] J.C. Caldero and P. Sahuc, Shaping amplifier designed at IPN Lyon.

[52] M. Goyot, Development of high speed low noise transimpedance preamplifier in bipolar technology, LYCEN 9535.

[53] M. Felcini et al., CMS Technical Note 94–252.

[54] M. Schneegans, Proc. XXVIth Rencontres de Moriond, Les Arcs, 1991, ed. J. Tran Thanh Van (Editions Frontières, Gif-sur-Yvette), p.473.

[55] CMS Technical Proposal, CERN-LHCC/94–38 (1994).

[56] M. Kobayashi et al., Nucl. Instrum. Methods Phys. Res. **A333** (1993) 429.

[57] P. Lecoq et al., Nucl. Instrum. Methods Phys. Res. **A365** (1995) 291.